Ore Geology Reviews 118 (2020) 103363

Contents lists available at ScienceDirect

Ore Geology Reviews

journal homepage: www.elsevier.com/locate/oregeorev

Molybdenite Re-Os dating and LA-ICP-MS trace element study of sulfide minerals from the Zijinshan high-sulfidation epithermal Cu-Au deposit, Fujian Province, China

Xiao-Yu Zhao[a,b], Hong Zhong[a,b,*], Wei Mao[a], Zhong-Jie Bai[a], Kai Xue[c]

[a] State Key Laboratory of Ore Deposit Geochemistry, Institute of Geochemistry, Chinese Academy of Sciences, Guiyang 550081, China
[b] University of Chinese Academy of Sciences, Beijing 100049, China
[c] Zijin Mining Group Co. Ltd, Shanghang 364200, China

ARTICLE INFO

Keywords:
High-sulfidation epithermal Cu-Au deposit
Molybdenite Re-Os age
Sulfides
In-situ trace elements
Zijinshan

ABSTRACT

The Zijinshan Cu-Au deposit, located in Fujian Province, is the largest high-sulfidation epithermal (HSE) deposit in Southeastern China and is usually regarded as a major part of the porphyry Cu system in the Zijinshan ore field. Molybdenite samples collected from the Cu mineralization zone yield a first weighted mean Re-Os age of 111.31 ± 0.70 Ma, which is explained as the time of dickite-alunite alteration. Combining the newly reported muscovite ^{40}Ar-^{39}Ar and zircon U-Pb ages (~113 Ma), the mineralization of Zijinshan is likely to initiate before ca. 110 Ma. This result is obviously older than the Re-Os age of the adjacent Luoboling porphyry Cu-Mo deposit (~105 Ma).

Pyrite, chalcopyrite, bornite, digenite, and covellite collected from the deep potassic, middle phyllic and upper epithermal zones are used to conduct LA-ICP-MS trace element analysis. The spatial zonings of mineralization and alteration and the regular variations of trace elements in sulfides at vertical direction imply a potentially complete transition from porphyry to epithermal mineralization and the deep origin of ore-forming fluids. Mineralogical and trace element characteristics indicate that the chalcopyrite formed in both stages, whereas bornite is the product of epithermal mineralization, rather than a porphyry stage residue. The majority of digenite and covellite has hypogene genesis. Pyrite and digenite in the epithermal zone are major carriers of primary Au. Au in pyrite is Te-Bi related and exists as solid solutions or different-sized telluride and Bi-sulfosalt inclusions. Compared to As, Te and Bi played more important roles to scavenge Au and Ag and achieve the primary Au enrichment. Differently, Au in digenite is independently locked in digenite lattice. Bornite and digenite are good carriers of primary Ag, which mainly exists as solid solutions. The high sulfidation state stage is the major period for concentrations of primary Au and Ag. The upward increase of Au in primary sulfides of HSE Cu zone implies that the distribution pattern of upper Au enrichment and lower Cu enrichment is not only caused by supergene process, but is also controlled by hypogene trend.

Based on the mineralization and alteration zonings, the spatial variation of trace elements and the presented Re-Os age, the ore-forming fluids of the Zijinshan Cu-Au deposit most likely originate from deep region, rather than from the adjacent Luoboling porphyry deposit. The Zijinshan and the Luoboling deposits should belong to two independent hydrothermal systems.

1. Introduction

The Zijinshan Cu-Mo-Au-Ag mineralization district, located in Fujian Province, southeastern China is well-known for its considerable metal reserves with over 399 t Au, 4.1 Mt Cu, 6339 t Ag and 0.11 Mt Mo (Zhang, 2013). This district hosts different deposit types, mainly including the Luoboling porphyry Cu-Mo deposit, Zijinshan high-sulfidation epithermal (HSE) Cu-Au deposit, Yueyang low-sulfidation epithermal (LSE) Ag polymetallic deposit and Wuziqilong transitional Cu deposit, constituting a complete porphyry-epithermal mineralization system (Jiang et al., 2013; Sillitoe, 2010; Xu et al., 2016; Zhang et al., 2001, 2005). Numerous studies have been conducted in recent decades on the geochronology, geology, geochemistry and fluid inclusion to reveal the origin of these ore deposits (e.g., So et al., 1998;

* Corresponding author at: State Key Laboratory of Ore Deposit Geochemistry, Institute of Geochemistry, Chinese Academy of Sciences, Guiyang 550081, China.
E-mail address: zhonghong@vip.gyig.ac.cn (H. Zhong).

https://doi.org/10.1016/j.oregeorev.2020.103363
Received 14 November 2019; Received in revised form 13 January 2020; Accepted 23 January 2020
Available online 27 January 2020

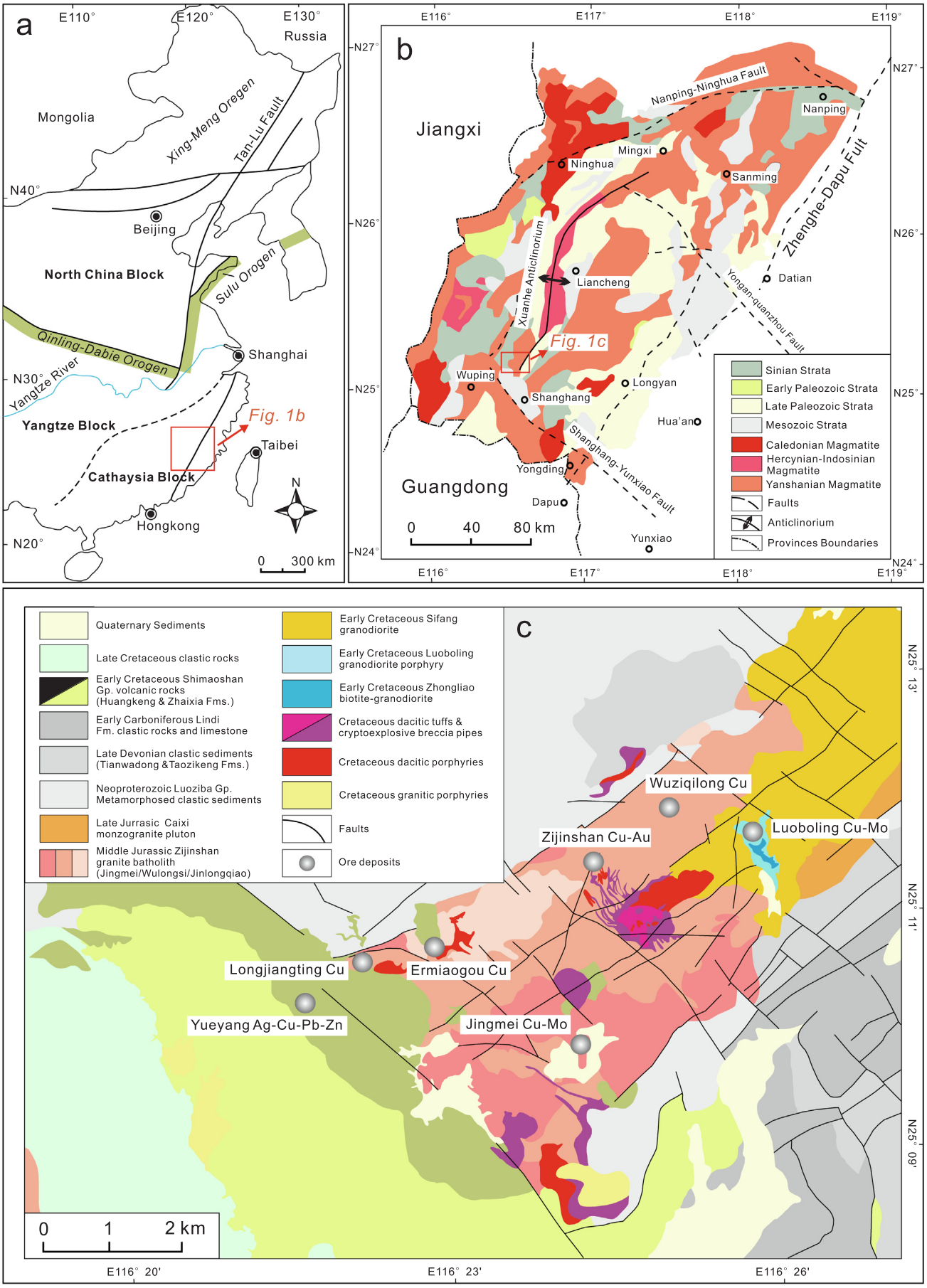

(caption on next page)

Fig. 1. (a) Simplified geological map of eastern South China (modified after Li et al. 2017). (b) Reginal geological map of Fujian Province (modified after Wu et al. 2017; Zhong et al. 2011). (c) Geological map of the Zijinshan ore field (modified after Pan et al., 2019 and unpublished data from Zijin Mining Group Co.).

Zhang et al., 2001, 2003, 2005; Li and Jiang, 2017; Jiang et al., 2013, 2015, 2017; Zhong et al., 2014, 2017, 2018; Wu et al., 2017, 2018; Xu et al., 2016; Piquer et al., 2017; Huang et al., 2018; Liu et al., 2016, 2017, 2019; Chen et al., 2019; Pan et al., 2019), especially the Zijinshan HS epithermal Cu-Au deposit with the largest metal reserves (305 t Au and 2.32 Mt Cu, Jiang et al., 2017). Drilling data shows that the HSE mineralization at Zijinshan reaches 1700 m depth below the surface (Zhang, 2013), whereas the typical porphyry ore bodies with economic value have still not been revealed. The genetic relationship between the Zijinshan HSE deposit and the adjacent Luoboling porphyry deposit is thus significant to guide further regional and deep exploration (e.g., Zhang et al., 2003; Zhong et al., 2014; Jiang et al., 2017; Li and Jiang, 2017; Huang et al., 2018; Pan et al., 2019). However, although the reported mineralization ages of the Luoboling deposit are uniform (molybdenite Re-Os age, ~105 Ma; Duan et al., 2017; Liang et al., 2012; Zhong et al., 2014; Li and Jiang, 2017), the mineralization ages of the Zijinshan deposit are still debatable, which directly prevents deciphering the genetic relationship between these two deposits. In the reported age data, some dating results obtained from the volcanic rocks and alteration minerals related to the mineralization yield ages younger than 110 Ma, mainly between 100 and 105 Ma (e.g., Chen, 1996; Zhang et al., 2003, 2005; Jiang et al., 2015, 2017; Hu et al., 2012; Pan et al., 2019), whereas several ages older than 110 Ma have also been reported (Zhang et al., 1991; Jiang et al., 2013; Huang et al., 2018). The recently reported muscovite ^{40}Ar-^{39}Ar and zircon U-Pb dating limited the mineralization age between 110 and 113 Ma (Huang et al., 2018), whereas the new alunite dating displays ^{40}Ar-^{39}Ar age between 101 and 103 Ma (Pan et al., 2019), implying a deviation caused by mineral selection. In the present study, molybdenite as an ideal dating mineral, was first selected to yield Re-Os age and restrict the mineralization time of the Zijisnhan Cu-Au deposit. In addition, the direct comparison of dating results acquired from same mineral and dating method, is achieved to provide more reliable evidence in judging the relationship between the Zijinshan and the Luoboling deposits.

Laser ablation inductively coupled plasma mass spectrometry (LA-ICP-MS) method provides a good opportunity to achieve trace element analysis in sulfide minerals. Numerous related studies on pyrites have been conducted in different Au deposits, such as the Carlin, orogenic and epithermal types, in which pyrite is utilized to investigate the mineralogical form and enrichment mechanism of Au (e.g., Reich et al., 2005; Cook et al., 2009, 2013; Zhang et al., 2014; Zhao et al., 2011; Deditius et al., 2014; Bi et al., 2011). Unfortunately, similar studies for pyrite and Cu-(Fe)-sulfides in porphyry-HSE systems are still limited (e.g., Franchini et al., 2015; Cook et al., 2011). The Au mineralization of the Zijinshan Cu-Au deposit is the result of supergene enrichment, in which the Au ores are generally presented as oxidation ores and the Au is hosted by oxide minerals such as limonite (So et al., 1998). The release and reprecipitation of Au from hypogene sulfides are important for supergene Au enrichment (Chen et al., 2019). However, the primary enrichment process of Au is still unclear. The lower hypogene HS Cu mineralization zone hosts 46 t associated Au and 2389 t associated Ag (Zhang, 2013), which has economic values and is significant to clarify the primary enrichment processes of Au and Ag. In this study, we systematically analyze pyrite and four major Cu-(Fe)-sulfide minerals collected from the deep potassic, middle phyllic and upper HS epithermal zones with a vertical range up to ~1500 m in the Zijinshan Cu-Au deposit, to clarify the distribution and enrichment processes of trace elements (especially Au and Ag) and to understand the genesis of different Cu-(Fe)-sulfide minerals. In combination of the above studies, the genetic relationship between the Zijinshan and Luoboling deposits was further discussed.

2. Geologic setting

2.1. Regional geology

The South China Block is divided into the Yangtze Block in the northwest and the Cathaysia Block in the southeast (Fig. 1a). Due to subduction of the paleo-Pacific plate beneath the Eurasian Plate, extensive Yanshanian magmatism and associated Cu-Au, Au-Ag, Pb-Zn and W-Sn mineralization occurred in the Cathaysia Block, southeastern coastal area of China (Mao et al., 2013). The Zijinshan Cu-Mo-Au-Ag mineralization district is located in the central area of the Cathaysia Block, southwestern Fujian Province, at the intersection of the Xuanhe Anticlinorium and the Shanghang-Yunxiao Fault (Fig. 1a, b) (Wang et al., 2009; Wu et al., 2017, 2018; Jiang et al., 2017; Zhang et al., 2003, 2005; Qiu et al., 2010; Wang and Jue, 2013). Sinian, Early Paleozoic, Late Paleozoic, Mesozoic strata and Caledonian to Yanshanian magmatic rocks are exposed in the area (Fig. 1b). NE-trending faults (e.g., Zhenghe-Dapu and Nanping-Ninghua Faults) and NW-trending faults (e.g., Shanghang-Yunxiao and Yongan-Quanzhou Faults) control the main structural framework (Fig. 1b).

Within the Zijinshan ore field, several deposits with different scales and geneses have been discovered, including the Zijinshan HSE Cu-Au deposit (So et al., 1998; Zhang et al., 2003, 2005), Luoboling and Jintonghu porphyry Cu-Mo deposits (Zhong et al., 2011, 2014; Xue and Ni, 2008; Li et al., 2016; Liang et al., 2012; Huang et al., 2013), Ermiaogou HSE Cu deposit (Li et al. 2013), Yueyang LSE Ag-Cu-Pb-Zn deposit (Zhong et al., 2017), and transition types (from porphyry to HSE), such as the Wuziqilong and Longjiangting Cu deposits (Chen et al., 2011, 2015). NE- and NW-trending faults also control the distribution of magmatic intrusions and strata in the ore field (Fig. 1c). Recent study indicate that the NE-striking faults were active prior to mineralization, NW-striking faults controlled the emplacement of veins, breccias and dacite dikes during mineralization, whereas ENE-striking faults associated with minor conjugate NNW-striking faults formed after mineralization (Chen et al., 2019).

The main lithostratigraphic units exposed in the ore field are the Neoproterozoic Louziba Group, Late Paleozoic clastic sediments, Early Cretaceous volcanic assemblages, and Quaternary alluvial sediments (Fig. 1c). The Louziba Group is composed of low-grade metamorphic shallow marine sediments, including two-mica schist, muscovite schist, phyllite, metasiltstone and metasandstone. The Late Paleozoic sediments include the Late Devonian Tianwadong, Taozikeng Formations and the Early Carboniferous Lindi Formation. These strata comprise coastal to shallow marine facies siltstone, sandstone and conglomerate, locally intercalated with marl and felsic tuff. The Early Cretaceous Shimaoshan Group comprises dacite, rhyolite, ignimbrite and tuff, with minor conglomerate intercalations, unconformably overlying the rocks described above (Fig. 1c) (Xu et al., 2016; Zhong et al., 2011, 2014, 2017).

The major magmatic rocks within the Zijinshan district include the Late Jurassic Caixi monzogranite pluton, Middle Jurassic Zijinshan granite batholith, and the Early Cretaceous Sifang granodiorite, Luoboling granodiorite porphyry and Zhongliao granodiorite (Fig. 1c). The Caixi pluton displays zircon U-Pb ages of 146–150 Ma (Yu et al., 2013; Zhao et al., 2008; Hu et al., 2012). The Zijinshan granite batholith is composed of three subunits, including the Jingmei, Wulongsi and Jinglongqiao plutons (So et al., 1998; Zhang et al., 2001; Yu et al., 2013). Based on the crosscutting relationships in the field and the reported U-Pb ages, the Zijinshan batholith was emplaced at 149–168 Ma (Zhang et al., 2001; Yu et al., 2013; Zhou and Chen, 1996; Zhao et al., 2008; Jiang et al., 2013). The Sifang pluton is one of the host rocks of the Luoboling Cu-Mo deposit with emplacement ages of 104–112 Ma

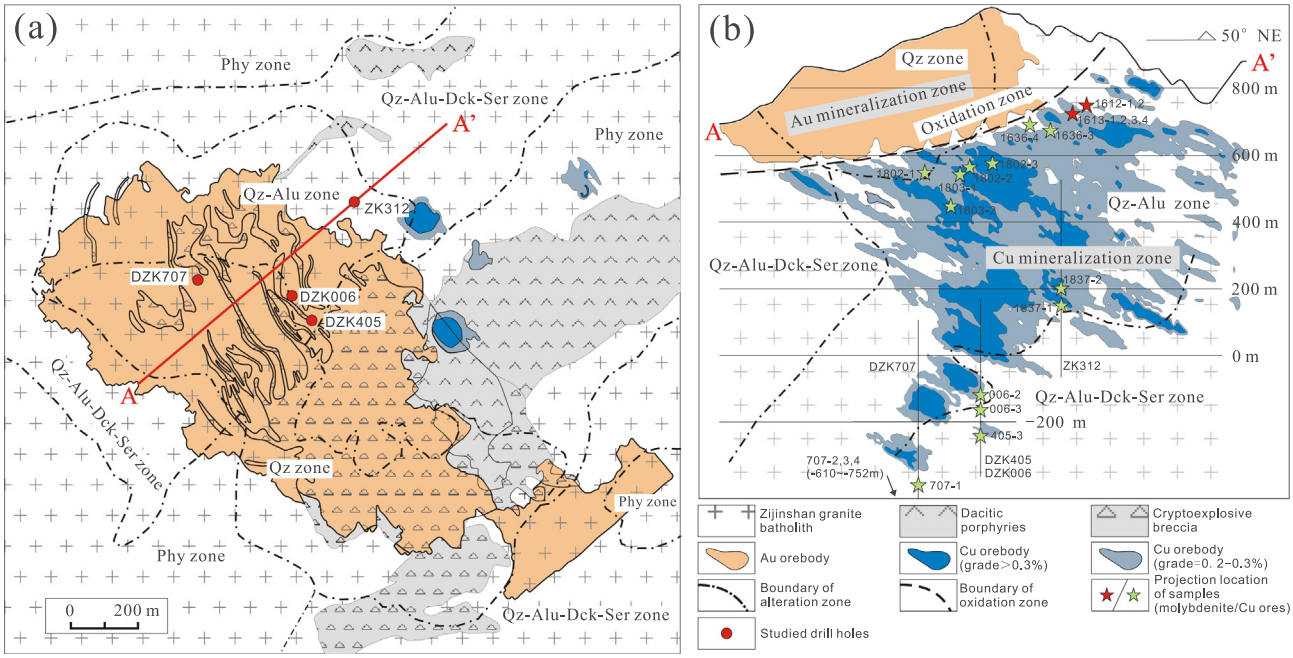

Fig. 2. (a) Simplified geological map and (b) cross-sectional profile of the Zijinshan high-sulfidation epithermal Cu-Au deposit (modified after Li et al. 2017; Zhong et al. 2018). The relative locations of colleted samples are projected on the section. *Abbreviations:* Qz zone = silicic alteration zone; Qz-Alu zone = quartz-alunite alteration zone; Qz-Alu-Dck-Ser zone = quartz-alunite-dickite-sericite alteration zone; Phy zone = phyllic alteration zone.

(Jiang et al., 2013; Hu et al., 2012; Mao et al., 2002; Yu et al., 2013). The Luoboling porphyry, spatially coexist with the Zhongliao pluton, is the most important ore-bearing porphyry in the Zijinshan district. They intruded the Sifang pluton with multistage ages ranging from 96 to 110 Ma (Huang et al., 2013; Liang et al., 2013; Yu et al., 2013; Li and Jiang, 2015, 2017). Small-scale Cretaceous cryptoexplosive breccia and dacitic porphyry closely associated with Cu-Au mineralization are widely scattered across the ore field (Fig. 1c).

2.2. Deposit geology

The Zijinshan HS epithermal Cu-Au deposit is located in the central area of the Zijinshan ore field, spatially associated with the Cretaceous pipelike dacite porphyry and surrounding cryptoexplosive breccia, tuff and lava (So et al., 1998; Wu et al., 2017; Li and Jiang, 2017; Fig. 1c, 2a). The Middle Jurassic Zijinshan granitic complex and the Cretaceous cryptoexplosive breccia and dacitic porphyry are host rocks of Cu-Au deposits. An upper oxidation, leaching zone, and a lower primary zone occur along the vertical direction, controlling the mineralization framework of Au enrichment in the upper part and Cu enrichment in the lower part (Jiang et al., 2017, Fig. 2b).

A series of alteration zones have been recognized from deep potassic alteration zone to upper HSE alteration zone. A mineral paragenesis in different mineralization and alteration zones is established in Fig. 3.

The potassic alteration is recognized in the recent deep drill hole DZK 707 at levels < −500 m, which is also mentioned by So et al. (1998) and Wu et al. (2017). This alteration type occurs as potassic granodiorite with massive and clustered K-feldspar overprinted by abundant quartz-molybdenite-chalcopyrite-pyrite veins (Fig. 4l). Quartz-molybdenite veins (Fig. 4k), K-feldspar-molybdenite-chalcopyrite-pyrite veins (Fig. 4m) and pure K-feldspar veins (Fig. 4n) are also usually observed. Fine-grained secondary (hydrothermal) biotite is discovered to coexist with abundant K-feldspar. The sulfide mineral association of molybdenite + chalcopyrite + pyrite is representative of this zone and displays mineralization features similar to those of typical porphyry deposits. The potassic alteration zone is partly overprinted by sericite alteration.

In contrast, the phyllic alteration zone that mainly contains quartz, sericite and pyrite is shallower and intensely overprinted by alunite and dickite (Figs. 2; 4h, i, j; So et al., 1998; Zhong et al., 2018; Li and Jiang, 2017; Wu et al., 2017). This zone is dominated by quartz-pyrite veins with abundant coarsely crystalline euhedral pyrite (Fig. 4i, j; 5b). Quartz-pyrite veins are usually cut by dickite veinlets (Fig. 4j). Limited HSE ore veins with a sulfide association of digenite + bornite + chalcopyrite + pyrite are also observed in this zone (Figs. 4h; 5e, f).

The increases of dickite and alunite upward and outward form the quartz-dickite-alunite-sericite alteration zone above the phyllic zone (Fig. 2b). Dickite is predominant in this zone and occurs as both alteration minerals and pure dickite veinlets. Sulfides are not abundant and only minor digenite and pyrite are discovered to distribute in dickite veins or altered rocks as disseminated grains (Fig. 4b).

The quartz-alunite alteration zone developed in the shallower and more central area compared with the quartz-alunite-dickite-sericite alteration zone. Alunite, quartz, pyrite, dickite and minor sericite are common. The HSE Cu ore bodies are mainly confined in this alteration zone (Fig. 2b). Copper ores occur as veins and veinlets with widths varying from several millimeters to tens of centimeters, filling or replacing hydrothermal breccia, altered granite and dacite porphyry (Fig. 4a, d). The species of metallic minerals are very abundant in this zone (Liu et al., 2016). Major ore minerals include digenite, covellite and enargite, whereas minor chalcocite, bornite and chalcopyrite also occur locally. In this study, four different sulfide associations are observed. (1) Digenite + bornite + chalcopyrite + pyrite (Figs. 4f; 5g). This association is similar to that in the HS veins of the phyllic zone. Bornite is seemingly replaced by massive digenite, whereas limited chalcopyrite mainly occurs as tiny granular crystals exsolved from bornite. (2) Digenite + covellite + pyrite (Fig. 4a, d). Digenite only coexists with covellite to form veins and covellite usually occurs as small foliated crystals exsolved from digenite (Fig. 5i) or coexists with covellite as interbeds (Fig. 5h). (3) Covellite + pyrite ± enargite. Tabular (Fig. 4g, 5j) or massive (Fig. 5k) covellite coexists with anhedral pyrite and enargite. Fine-grained covellite fragments were also observed to disperse between gangue minerals as clusters together with fine-grained euhedral pyrite (Fig. 5d). (4) Enargite + secondary covellite + pyrite. This association occurs only at the top of the Cu mineralization zone. Secondary covellite replaces enargite along the

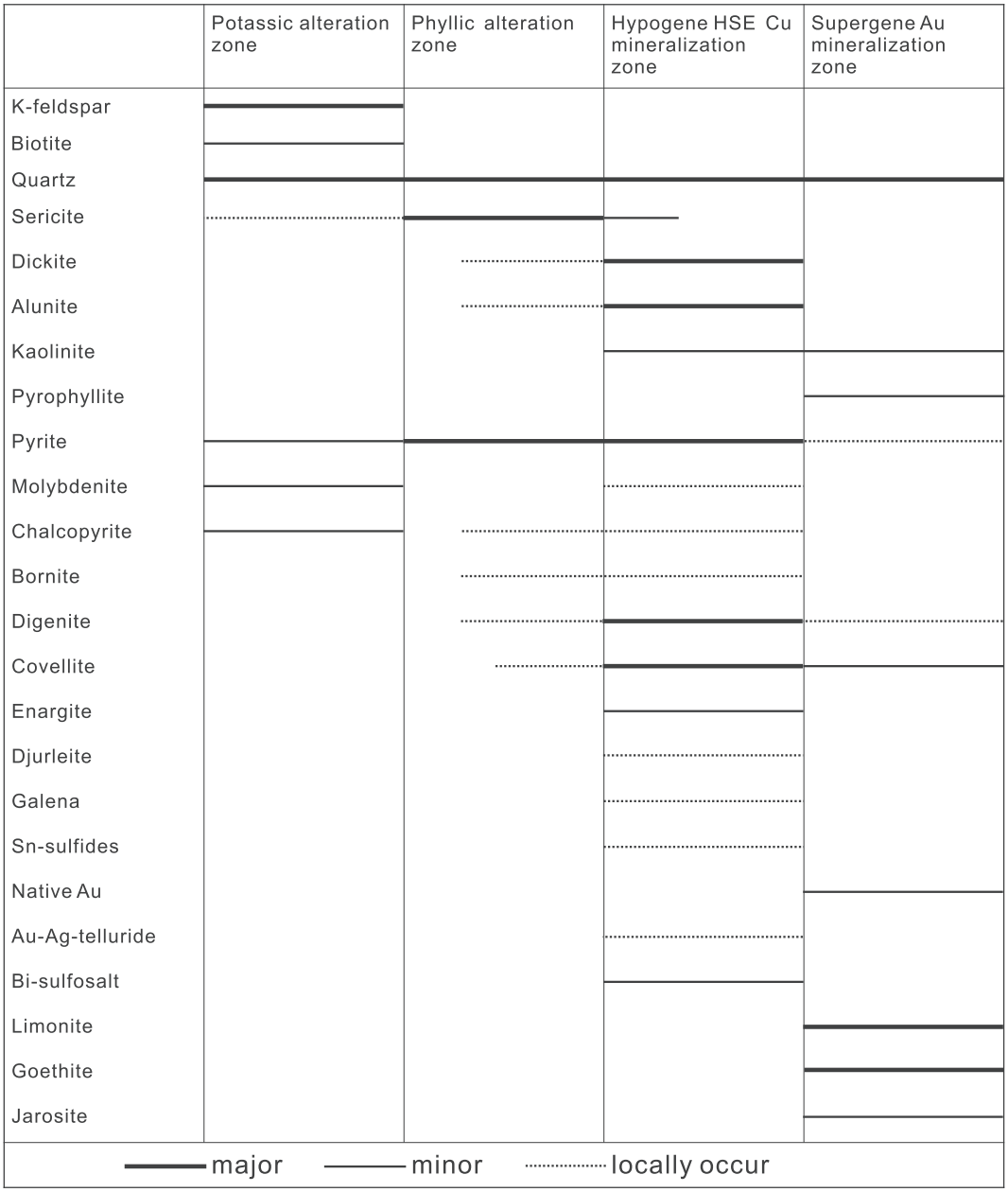

Fig. 3. Paragenetic sequence of ore and gangue minerals from the different alteration and mineralization zones in the Zijinshan deposit.

mineral margin (Fig. 5l) or coexists locally with fine-grained pyrite clusters. Compared with primary covellite, secondary covellite is obviously anhedral, as well as rougher and dirtier under the microscope. Molybdenite is not abundant but can also be locally observed in this zone. In the field, molybdenite ores display massive or vein structure, locally crosscut alunite-dickite-quartz altered granite and dacite porphyry. Molybdenite and dickite also locally constitute molybdenite-dickite veinlets in advanced argillic rocks. The molybdenite grains are presented as thin-skinned, veinlet-like or disseminated aggregates. Pyrite, dickite, alunite and coarse-grained quartz are abundant in hand specimens (Fig. 6b, c, d).

Intense silicic alteration zone is dominant in the upper part of the deposit, like a hat-shaped surficial cap, as a result of acid leaching and supergene oxidation (Fig. 2b). This zone is characterized by abundant quartz (> 90%) and minor limonite, goethite, jarosite, dickite, and kaolinite. Gold has been supergene-enriched during weathering forming a quartz-limonite-native gold assemblage. Gold ore bodies are strictly confined by the silicic and oxidation zone above a nearly +600 m elevation level (Jiang et al., 2017). The Au ores are mainly controlled by fractures and hydrothermal breccia, in which the fragments are mostly composed of silicified granite and dacite porphyry (Zhong et al., 2018). Vuggy quartz is the dominant gangue mineral in Au ores, but minor clay minerals such as dickite and rare alunite and sericite also appear. Limonite and goethite are the main Au-bearing minerals (So et al., 1998).

3. Samples and methods

3.1. Samples

Nineteen samples picked from 63 ores collected from the open pit and drill cores ZK 312, DZK 405, DZK 006 and DZK 707 in the Zijinshan Cu-Au deposit were used to make slices and launch LA-ICP-MS in situ geochemical analysis of sulfide minerals. The sampling locations cover ~1500 m in the vertical direction from −752 m to +700 m elevation, for all of the potassic, phyllic, HSE alteration zone and related sulfide

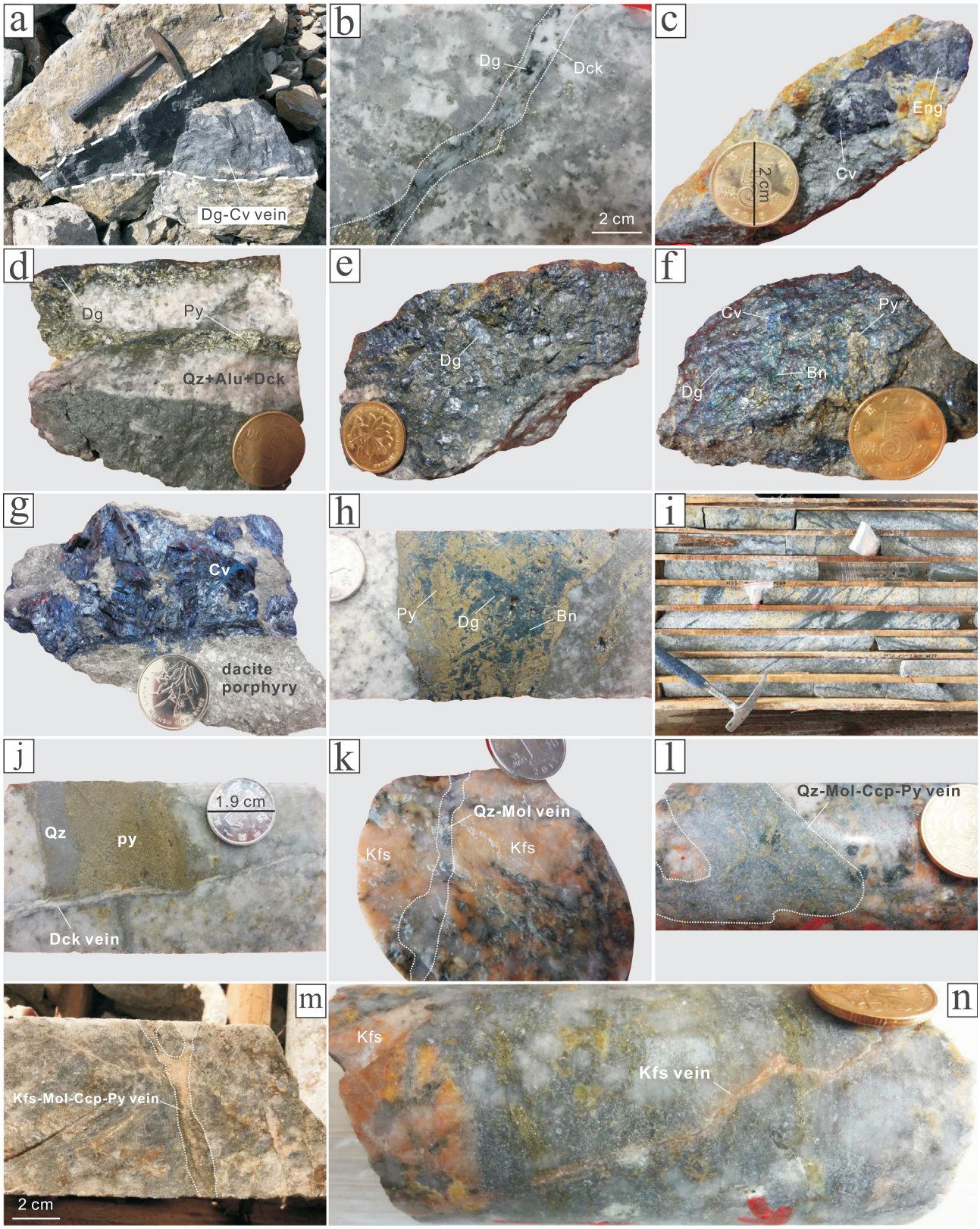

Fig. 4. Ores and associated alteration types in the Zijinshan deposit. (a) Digenite-covellite vein cuts the Zijinshan granite with advanced argillic alteration. (b) Dickite-digenite-pyrite vein in dickite-quartz alteration zone. (c) Isolated residue of enargite and secondary covellite in silicic alteration rock. (d) Centimeter-wide digenite-pyrite veins cut quartz-alunite-dickite altered granite. (e) Aggregate of tabular digenite. (f) Massive digenite ore contains scattered fine-grained bornite and covellite grains. (g) Tabular primary covellite in altered dacite porphyry. (h) Digenite-bornite-pyrite vein in the phyllic alteration zone from drill cores with ~−180 m elevation. (i) Phyllic altered granite with abundant pyrite veins (~−360 m elevation). (j) Pyrite-quartz vein associated with phyllic alteration cut off by later dickite veinlet (~−250 m elevation). (k) Quartz-molybdenite vein in potassic granodiorite in the deepest drill cores (~−750 m elevation). (l) Quartz-molybdenite-chalcopyrite-pyrite vein in potassic granodiorite. (m) K-feldspar-molybdenite-chalcopyrite-pyrite vein in the potassic zone. (n) Pure K-feldspar vein cuts sulfide-bearing quartz vein. *Abbreviations:* Dg = digenite; Cv = covellite; Eng = enargite; Bn = bornite; Ccp = chalcopyrite; Mol = molybdenite; Py = pyrite; Qz = quartz; Alu = alunite; Dck = dickite; Kfs = K-feldspar.

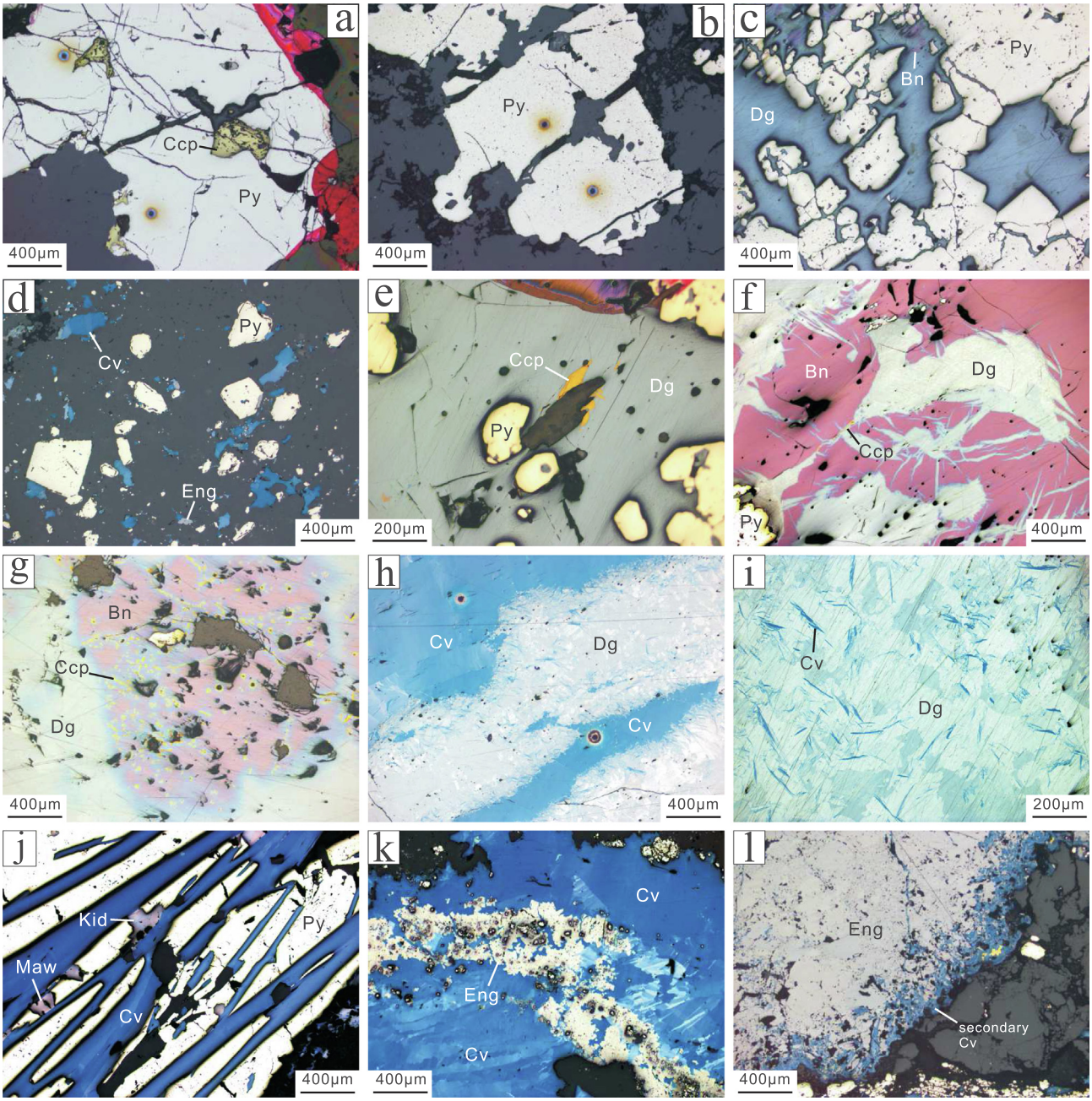

Fig. 5. Photomicrographs of major sulfides from different alteration zones showing different textures and genesis. (a) Chalcopyrite surrounded by coarse-grained euhedral pyrite in the Qz-Mol-Ccp-Py veins of the potassic alteration zone. (b) Coarse-grained pure euhedral pyrite in the phyllic alteration zone. (c) Medium-grained subhedral pyrite coexisting with digenite in the HS Cu mineralization zone. (d) Fine-grained euhedral pyrite scattered across the gangue minerals together with covellite and enargite. (e) Subrounded pyrite and isolated irregular chalcopyrite in massive digenite. (f) Bornite within massive digenite presenting fragmentary and bay-like textures. (g) Bornite with fine-grained chalcopyrite exsolution replaced by digenite. (h) Primary covellite and digenite constituting interbeds. (i) Foliated covellite crystals exsolved from digenite. (j) Columnar euhedral primary covellite intertwining with anhedral pyrite and W, Sn-bearing minerals. (k) Primary massive covellite coexisting with enargite. (l) Enargite replaced by secondary covellite along the mineral margin. *Abbreviations:* Py = pyrite; Ccp = chalcopyrite; Bn = bornite; Dg = digenite; Cv = covellite; Eng = enargite; Kid = Kiddcreekite; Maw = Mawsonite.

mineral assemblages described above. The relative locations of the studied drill holes and samples are illustrated in Fig. 2. Six molybdenite samples used for Re-Os isotope dating are collected from the mining platforms at +748 m to +720 m elevations in the southeastern corner of the open pit (Figs. 2b, 6a), which is located in the upper part of the primary Cu mineralization zone.

3.2. Methods

Molybdenite concentrated parts were cut from samples and crushed to 60–80 mesh, and then molybdenite grains were handpicked under a binocular microscope for three times to ensure purity over 99%. Re-Os isotope analysis was performed at the Re-Os Laboratory, National Research Center of Geoanalysis, Chinese Academy of Geological Sciences (CAGS) in Beijing, using a TJA X-series ICP-MS instrument. Detailed analytical procedures were described by Du et al. (1994, 2004). The ^{187}Re decay constant of 1.666×10^{-11} $year^{-1}$ (Smoliar et al., 1996) was used to calculate model ages, and the confidence level of model ages was 95%. The actual tested model age of molybdenite standard GBW04435 in our analysis was 222.2 ± 3.4 Ma, which is

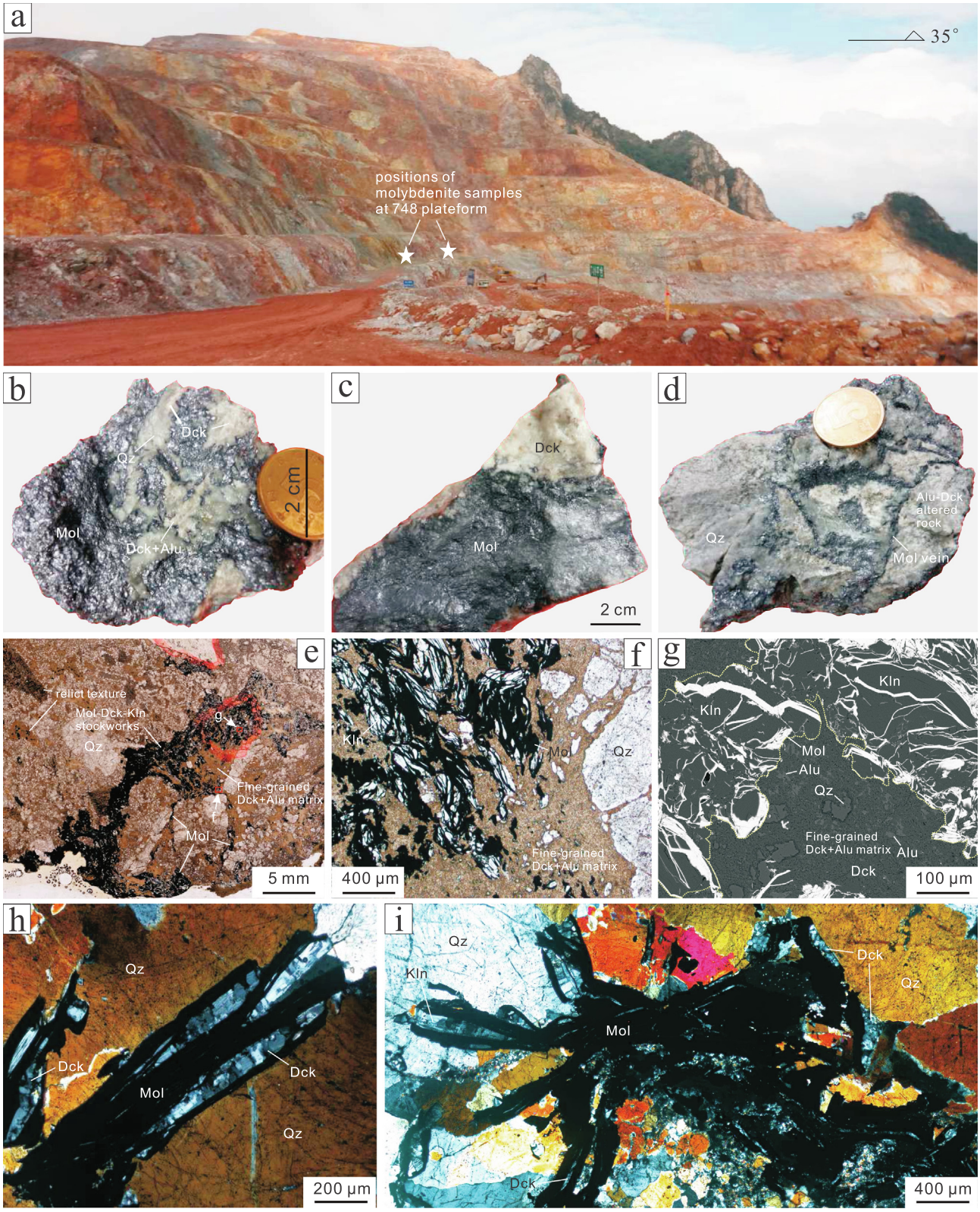

Fig. 6. (a) The +748 m platform where molybdenite samples were collected. (b) Massive molybdenite ore showing molybdenite coexists with dickite, alunite and coarse-grained quartz. (c) Thin-skinned molybdenite coexist with pure dickite. (d) Molybdenite veins crosscut alunite-dickite altered rock. (e) Molybdenite, dcikite and kaolinite constitute skockworks, confined in fine-grained dickite-alunite matrix, together replaced protolith and locally formed relict texture. (f) Cogenetic molybdenite and kaolinite grow together in alunite-dickite matrix. (g) Cogenetic molybdenite and kaolinite grow tegether in alunite-dickite matrix under BSE. Note the abundant alunite grains in matrix. (h) Cogenetic molybdenite and dickite in coarse-grained quartz. Well-crystallized dickite exclusively grow together with molybdenite graines. (i) Cogenetic molybdenite-dickite-kaolinite association crosscut coarse-grained quartz. *Abbreviations:* Mol = molybdenite; Qz = quartz; Dck = dickite; Alu = alunite; Kln = kaolinite.

identical to the standard value of 221.4 ± 5.6 Ma (Du et al., 2004).

Digenite, covellite, bornite and chalcopyrite, as four major Cu-carrying ore minerals in this deposit, were analyzed together with pyrite. Major and trace element analyses by LA-ICP-MS were performed at the State Key Laboratory of Ore Deposit Geochemistry, Institute of Geochemistry, Chinese Academy of Science (IGCAS) in Guiyang. The methodology outlined by Danyushevsky et al. (2011) was followed. Laser sampling was performed using a NWR-213 laser ablation system (New Wave Research, ESI United Kingdom Electro Scientific Industries Europe Ltd, Huntingdon, Cambridge, UK). An Agilent 7700x ICP-MS instrument was used to acquire ion-signal intensities. Helium (480 ml/min) was applied as a carrier gas. Argon (900 ml/min) was used as the make-up gas and mixed with the carrier gas via a Y-connector before entering the ICP. Each analysis incorporated a background acquisition of approximately 30 s (gas blank) followed by 60 s of data acquisition from the sample. Analyses were run with a 25 μm pit size, 10 Hz pulse frequency and 3.5 J cm^{-2} fluence. The internal standard Py was used to calibrate the concentrations of S and Fe. The integrated count data of concentrations for other elements were calibrated and converted by GSE-1G and GSD-1G. The preferred values of element concentrations for the USGS reference glasses were from the GeoReM database (http://georem.Mpch-mainz.gwdg.de). The sulfide reference material MASS-1 (Wilson et al., 2002) was analyzed as an unknown sample to check the analytical accuracy. The following isotopes were monitored: ^{29}Si, ^{34}S, ^{51}V, ^{55}Mn, ^{57}Fe, ^{59}Co, ^{60}Ni, ^{65}Cu, ^{75}As, ^{77}Se, $^{107,109}Ag$, ^{115}In, ^{118}Sn, ^{121}Sb, ^{125}Te, ^{184}W, ^{197}Au, ^{208}Pb and ^{209}Bi. The stabilization of major elements in five analyzed sulfides proved by a large amount of electron microprobe analyses allowed us to use Fe and Cu to conduct the internal standardization of pyrite and Cu-(Fe)-sulfides, respectively. The LADR software (http://norris.org.au/ladr/) was used to achieve data reduction.

4. Results

4.1. Molybdenite Re-Os age

Six molybdenite separates from samples collected in the Zijinshan Cu-Au deposit yield individual Re-Os model ages ranging from 109.5 ± 2.4 Ma to 111.9 ± 1.7 Ma, showing excellent reproducibility (Table 1). These results give a weighted mean age of 111.31 ± 0.70 Ma, with a MSWD of 0.77 at the 2σ level (Fig. 7). Extremely low contents of common Os (Table 1, $^{187}Os/Os \approx 100{,}000$) imply near-zero initial values of ^{187}Os, indicating that the mean weighted model age of 111.31 ± 0.70 Ma could represent the crystallization age of molybdenite.

4.2. LA-ICP-MS data for sulfides

The results for LA-ICP-MS spot analyses of pyrite (112), chalcopyrite (37), bornite (53), digenite (75) and covellite (38 for primary genesis and 11 for secondary genesis) are summarized in Table 2. Full details of the dataset are given in Supplementary Appendix A. Representative LA-ICP-MS time-resolved profiles are shown in Fig. 8.

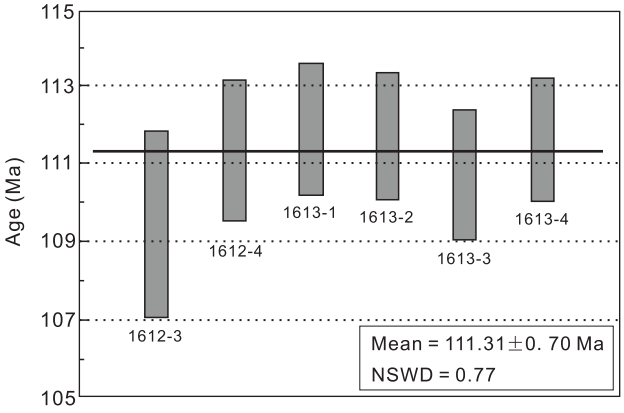

Fig. 7. Molybdenite Re-Os weighted average model age diagram.

In the potassic alteration zone, pyrite grains from quartz-molybdenite -chalcopyrite-pyrite veins (Fig. 5a) are depleted in most trace elements but enriched in Co (up to 3880 ppm), Ni (193 ppm) and Se (up to 73.2 ppm). Chalcopyrite grains (Fig. 5a) are enriched in V (up to 161 ppm), Mn (up to 118 ppm), Se (up to 100 ppm) and In (up to 115 ppm), which are obviously higher than the values for chalcopyrite in HS veins. Several to tens of ppm Ag, Co, Ni, Pb and Bi have also been detected.

Pyrite in quartz-pyrite veins from the phyllic zone (Fig. 5b) display trace elements similar to those of pyrite in the potassic zone, except for higher Pb (up to 494 ppm) and Bi (up to 227 ppm), as well as lower Co (< 80 ppm) and Ni (< 20 ppm). In the HS epithermal veins of the phyllic zone, pyrite (Fig. 5e) shows significant enrichment in most trace elements compared with pyrite in the potassic zone and quartz-pyrite veins in the phyllic zone, including higher Au (up to 2.2 ppm), Ag (up to 34 ppm), W, Te, Pb and Bi (Table 2). The Co and Ni contents are similar to those in pyrite in the quartz-pyrite veins of the phyllic zone but lower than those in the potassic zone, only Se presents entirely lower values. Fine-grained chalcopyrite in HS epithermal veins (Fig. 5e) exhibits completely different trace elements from chalcopyrite in the deeper potassic zone, with higher Au (up to 5.3 ppm), Pb (up to 211 ppm), Bi (up to 55.6 ppm) and general decreases in most other elements (V, Mn, Se and In). Bornite (Fig. 5f) in HS veins is characterized by the highest content of Bi (up to 546 ppm) in all sulfides. Digenite (Fig. 5e) has Au (< 1 ppm) and Ag (< 40 ppm) concentrations obviously lower than shallower digenite. Several to tens of ppm Se and Pb, as well as Bi that are lower than only bornite, have also been obtained.

The HSE Cu mineralization zone in the shallow part possesses the most abundant trace elements. Pyrite in this zone (Fig. 5c, d) exhibits the highest Au contents of all sulfides (up to 12.1 ppm) and the highest Ag (up to 64 ppm) and Te (up to 26 ppm) in all pyrite types. Bornite in this zone (Fig. 5g) displays trace elements similar to those in the HS veins of the phyllic zone (Fig. 5f), apart from higher contents of Ag (up to 124 ppm) and Se (up to 66 ppm) and lower contents of Bi. Digenite in this zone is characterized by high and stable values of Au (up to 2.9 ppm) and the highest contents of Ag (up to 464 ppm) for all primary

Table 1
Re-Os isotope data for molybdenite from the Zijinshan Cu-Au deposit.

Sample no.	Weight (g)	Re (ppb)		Os_{common} (ppb)		^{187}Re (ppb)		^{187}Os (ppb)		Age (Ma)	
		content	2σ	content	2σ	content	2σ	content	2σ	value	2σ
ZJ 1612-3	0.01065	170810	3127	0.0007813	0.0426347	107358	1965	195.9	1.3	109.5	2.4
ZJ 1612-4	0.01168	177438	1911	0.002898	0.065991	111523	1201	207.1	1.4	111.4	1.8
ZJ 1613-1	0.01010	173350	1715	0.003332	0.110369	108954	1078	203.3	1.2	111.9	1.7
ZJ 1613-2	0.01009	184439	1675	0.003336	0.043075	115924	1053	216.0	1.3	111.8	1.6
ZJ 1613-3	0.01042	170876	1720	0.003226	0.141321	107399	1081	198.3	1.2	110.7	1.7
ZJ 1613-4	0.01011	173460	1462	0.003336	0.110664	109023	919	203.0	1.2	111.6	1.6

Table 2
Mean concentrations of major trace elements in sulfides determined by LA-ICP-MS (ppm) from the Zijinshan Cu-Au deposit.

Minerals	Sample (n)	ASL (m)	Occurrence	Au	Ag	V	Mn	Co	Ni	As	Se	In	Sb	Te	W	Pb	Bi
Py	707–3(10)	−752	Qz-Mol-Ccp-Py veins in the potassic zone	0.01	0.10	0.01	0.19	24.4	16.4	0.17	13.9	–	–	0.10	–	3.6	1.3
	707–2(10)	−629		–	1.2	0.04	0.41	1533	4.9	0.11	35.0	0.01	0.01	0.07	–	2.9	0.44
	707–4(8)	−610		–	0.25	–	0.18	429	81.1	–	13.2	0.02	–	–	0.03	0.58	0.71
	707–1(10)	−360	Qz-Py veins in the phylllic zone	0.01	0.60	–	1.5	4.5	1.3	–	5.9	0.003	0.02	0.11	–	3.5	2.8
	405–3(10)	−250		–	1.4	0.14	1.7	12.7	3.4	1.8	12.0	0.06	0.11	0.62	0.01	86.4	28.2
	006–3(9)	−185	HS veins in the phyllic zone	0.34	7.0	0.59	2.4	10.4	7.9	3.3	2.2	0.80	1.5	1.9	23.0	65.6	200
	006–2(14)	−155		0.57	6.9	5.5	0.14	1.7	1.4	2.5	1.9	0.03	0.23	1.6	6.5	149	42.8
	1637–2(14)	200	HS Cu ores in the epithermal Cu	1.10	7.0	0.02	1.8	3.0	1.7	0.47	1.7	0.11	0.47	1.3	0.36	317	16.6
	1803–1(10)	550	mineralization zone	2.31	17.5	2.6	0.61	122	31.1	56.8	6.1	0.12	10.6	6.3	1.4	46.6	18.8
	1802–2(10)	570		3.88	16.6	17.4	74.7	287	135	25.9	2.3	0.19	2.1	4.9	24.5	252	50.6
	1636–4(7)	700		1.66	15.5	–	2.5	0.95	1.7	3.8	4.6	0.02	0.25	5.0	0.13	72.2	17.8
Ccp	707–3(8)	−752	Qz-Mol-Ccp-Py veins in the potassic zone	–	5.3	36.4	15.6	–	–	–	37.1	7.1	0.63	0.26	2.7	11.3	14.0
	707–5((8)	−650		–	7.2	1.6	18.3	1.2	0.23	–	48.0	4.9	0.70	0.51	0.81	6.5	0.86
	707–2(11)	−629		–	16.3	5.0	10.5	10.1	5.5	0.18	24.3	76.7	1.0	0.54	0.73	40.5	35.3
	006–2(0)	−155	HS vein in the phyllic zone	1.38	13.5	0.13	0.65	–	0.02	0.52	12.3	1.4	0.76	0.19	4.4	60.3	36.1
Bn	006–1(15)	−180	HS vein in phyllic zone	0.06	40.0	0.16	0.11	–	0.13	0.33	29.7	0.10	0.47	–	2.0	21.3	255
	006–2(9)	−155		–	40.2	–	–	–	–	–	32.9	0.09	0.14	–	0.14	16.1	437
	1636–3(5)	680	HS Cu ores in the epithermal Cu	0.02	70.6	0.04	0.14	–	–	–	41.3	0.09	–	0.11	0.01	12.7	153
	1636–4(14)	700	mineralization zone	0.08	71.0	–	0.11	–	–	0.08	41.8	0.20	0.01	0.13	–	26.3	147
Dg	006–1(15)	−180	HS vein in phyllic zone	0.13	23.8	–	–	–	–	–	11.3	1.2	0.05	0.27	–	18.3	82.9
	006–2(10)	−155		0.21	28.6	–	–	–	–	0.17	15.7	0.77	0.80	0.78	–	58.5	128
	1803–2(10)	450	HS Cu ores in epithermalCu mineralization	0.54	150	0.02	–	–	–	0.30	31.9	0.05	0.02	0.06	0.08	8.7	28.5
	1803–1(10)	550	zone	0.74	165	–	1.9	–	–	0.16	17.9	0.05	0.03	3.2	0.01	25.7	118
	1802–3(10)	578		1.07	203	–	9.4	–	–	0.27	34.7	0.14	0.02	0.27	0.02	58.0	182
	1636–3(10)	680		1.53	309	–	–	0.01	–	–	14.9	0.39	–	0.15	0.02	173	36.3
	1636–4(10)	700		1.13	193	–	0.54	–	–	–	13.9	1.4	0.06	0.07	0.04	210	100
Cv	1637–1(9)	175	HS Cu ore in epithermal Cu mineralization	0.21	4.9	0.05	0.16	0.07	0.19	26.1	15.9	0.52	1.5	24.9	6.4	16.9	7.4
	1637–2(7)	200	zone	0.22	3.4	0.02	–	0.04	0.12	7.2	18.2	0.01	0.52	25.6	0.02	5.7	2.9
	1803–1(10)	550		0.29	13.0	0.03	–	–	–	2.6	54.0	0.10	2.6	30.6	–	15.1	1.6
	1802–1(12)	560		0.01	12.7	–	–	–	–	1.2	63.1	0.01	0.18	12.8	0.01	3.9	0.56
	1625(11)	700	Secondary covellite	1.30	1558	24.6	1.1	–	0.07	902	3.6	5.6	35.6	0.31	58.2	151	19.0

n = number of individual spot analyses.
ASL = elevation of samples above sea level.
'–' = below the detection limits.

sulfides. Pb (up to 474 ppm) and Bi (up to 326 ppm) are also prominent compared with other Cu-(Fe)-sulfides. Primary covellite (Fig. 5h-k) only displays a weak ability to carry Au (generally < 0.5 ppm), Ag (generally < 20 ppm), Pb (generally < 40 ppm), As (generally < detection limits) and Bi (generally < 20 ppm) but prefers to incorporate Te (up to 120 ppm) and Se (up to 169 ppm). Secondary covellite (Fig. 5l) exhibits dramatic differences compared with primary covellite, mainly including anomalous enrichments in Ag (up to 2033 ppm), V (up to 142 ppm), As (up to 3550 ppm), Sb (up to 98 ppm) and W (up to 347 ppm), as well as common enrichments in Au (generally > 1 ppm) and Pb. Wide variation ranges of V, In, Sb, W and Pb imply the influence of mineral inclusions. Selenium and Te are only two elements with lower contents than those in primary covellite.

5. Discussion

5.1. Molybdenite Re-Os age

On the basis of Back scattered electron imaging (BSE), Energy spectrum, Raman spectrum analyses and the observations under the microscope, two different occurrences of molybdenite were recognized. In two samples (Fig. 6c), molybdenite, dickite and kaolinite constitute stockworks, or dispersedly distribute within fine-grained dickite-alunite matrix in alunite-dickite-quartz altered rocks (Fig. 6e, f, g). These molybdenite-dickite-kaolinite stockworks are strictly confined in matrix and never cut the coarse-grained quartz, indicating that the molybdenite-dickite-kaolinite stockworks are contemporaneous with fine-grained dickite and alunite. They together replaced protolith and locally formed relict textures (Fig. 6e). In other four samples (Fig. 6b, d), the mineral association of molybdenite + dickite + kaolinite directly occurs in or crosscuts coarse-grained quartz and alunite-quartz altered rock (Fig. 6h, i). Abundant kaolinite and dickite exclusively grow together with almost every molybdenite grains in all collected samples (Fig. 6e-i). These kaolinite and dickite grains are well-crystallized along the crystal direction of molybdenite, never crosscut molybdenite grains and are not discovered to coexist with any other minerals, indicating that these dickite and kaolinite are not formed by later hydrothermal superimposition, but are cogenetic with molybdenite. The cogenetic dickite and kaoliniate, as well as the contemporaneous fine-grained alunite indicate that the molybdenite dated in this study is the product during HSE mineralization process. The acquired Re-Os age can represent the time of epithermal mineralization event.

A lot of age data have been reported in the Zijinshan Cu-Au deposit (Table 3), mainly based on K-Ar or ^{40}Ar-^{39}Ar dating of altered minerals such as alunite and muscovite (Zhang et al., 1991, 1992, 2003; Zhou and Chen, 1996; Huang et al., 2018; Pan et al., 2019), Re-Os dating of pyrite (Jiang et al., 2017) and zircon U-Pb dating of (sub)volcanic rocks that related to the mineralization such as dacite, dacite porphyry, tuff and ignimbrite (Duan et al., 2017; Hu et al., 2012; Jiang et al., 2013; Pan et al., 2019; Huang et al., 2018; Yu et al., 2013). Some previous results are younger than 110 Ma (e.g., Zhang et al., 1992, 2003; Jiang et al., 2013, 2017; Hu et al., 2012; Duan et al., 2017; Pan et al., 2019). However, several ages older than 110 Ma (ranging from 111 to 113 Ma) have also been reported (Zhang et al., 1991; Jiang et al., 2013; Huang et al., 2018). In this study, molybdenite samples collected in the HS Cu mineralization zone yield weighted mean Re-Os age of 111.31 ± 0.70 Ma. This result is consistent with those obtained by Zhang et al. (1991) and Jiang et al. (2013) for alunite (K-Ar method, 111.7 Ma) and volcanic rocks (zircon U-Pb method, up to 111 Ma), but is ~8 Ma older than newly reported alunite ^{40}Ar-^{39}Ar ages (101–103 Ma; Pan et al., 2019). Huang et al. (2018) reported a ^{40}Ar-^{39}Ar age (113.4 ± 1.1 Ma) for muscovite that is cogenetic with dickite and a new zircon U-Pb age for ore-bearing volcanic breccia (112.9 ± 1.2 Ma), limited the Cu-Au mineralization time between

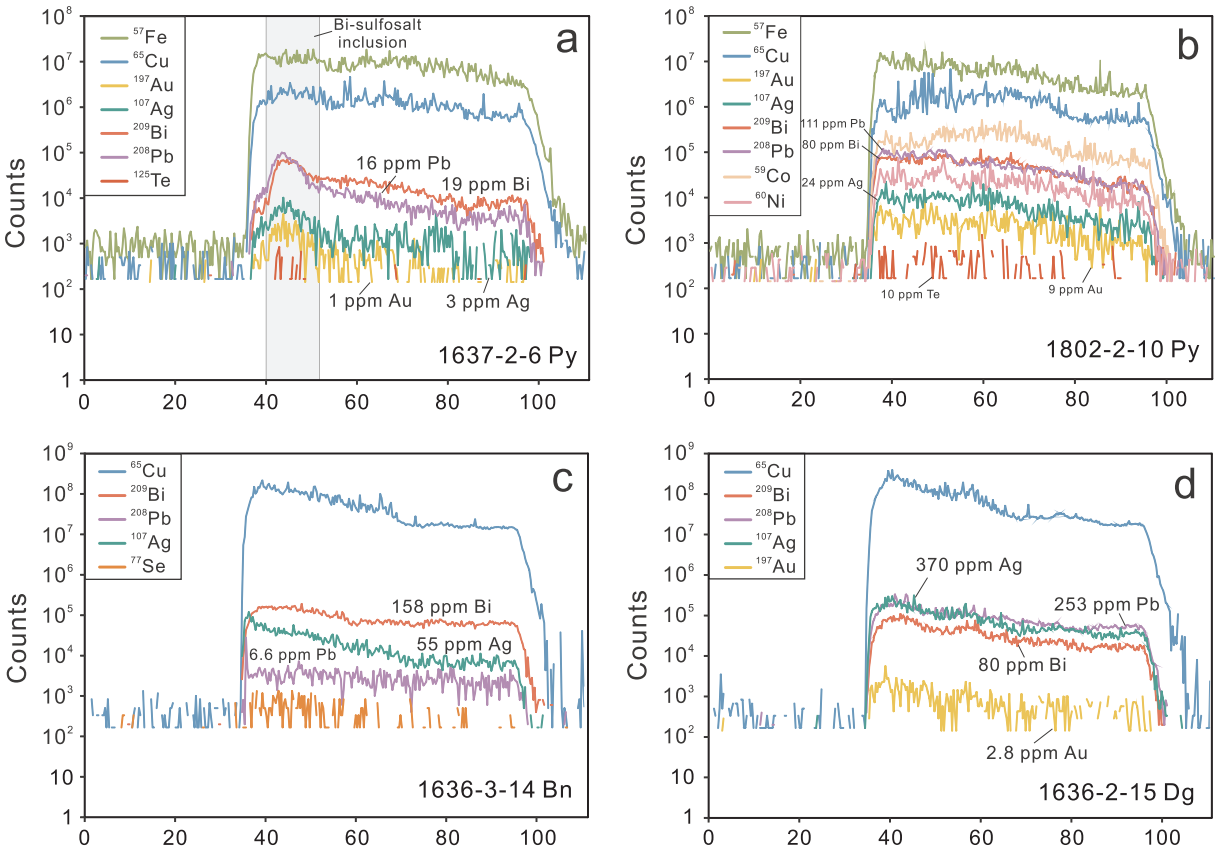

Fig. 8. Representative time-resolved LA-ICP-MS depth profiles of selected trace elements in sulfide minerals. From left, the background count is 35 s, followed by 60 s ablation time. (a) Pyrite with peaks of Pb, Bi, Au and Ag reflecting Bi-sulfosalt inclusion. (b) Pyrite with rough spectra. (c) Bornite with smooth spectra. (d) Digenite with smooth spectra and unnoticeable peaks of Pb, Bi, Au and Ag.

110 Ma and 113 Ma based on the crosscutting relationship of veins. Their dating results are very close to our molybdenite Re-Os age. The formation of advanced argillic alteration lithocap is testified usually prior to Au-Cu precipitation (Hedenquist et al. 1998, 2000; Heinrich et al. 2004; Heinrich, 2005; Sillitoe. 2010). The absence of coexisting Cu-sulfides in our molybdenite samples and the cogenetic relationship between molybdenite and dickite, kaolinite and alunite imply that the Re-Os age of ~111 Ma more likely represents the time of dickite-alunite alteration during advanced argillic alteration stage, which is slightly earlier but close to the Cu-Au mineralization. Combining the recently reported muscovite ^{40}Ar-^{39}Ar and Zircon U-Pb ages that up to 113 Ma (Huang et al., 2018), the mineralization of the Zijinshan deposit is likely to initiate before ca. 110 Ma. The age of ~111 Ma is consistent with the intrusion time of the adjacent Sifang granodiorite pluton (~112 Ma, Jiang et al., 2013), implying the potential genetic relationship at depth. Considering the large span of reported age data (up to 10 Ma), the possibility of episodic and prolonged multistage magmatic-hydrothermal activities can also not be eliminated in the Zijinshan deposit, on the conditions that all reported ages are precise and the ^{40}Ar-^{39}Ar system had not been reset by later magmatic and hydrothermal event. In addition, the evident ^{40}Ar-^{39}Ar age gap between alunite and muscovite emphasizes the influence of selected dating minerals on dating results in epithermal mineralization environment with low temperature, especially in deposits older than 100 Ma. The influence caused by different mineral closure temperatures should be further considered.

A possible genetic relationship between the Zijinshan epithermal Cu-Au deposit and the neighboring Luoboling porphyry Cu-Mo deposit (the only typical porphyry deposit in the ore field) has always been emphasized and used to guide further regional and deep exploration (e.g., Zhang et al., 2003; Zhong et al., 2014; Jiang et al., 2017; Li and Jiang, 2017; Huang et al., 2018; Pan et al., 2019). Direct comparison of molybdenite Re-Os ages between these two deposits eliminates the deviation caused by selection of dating minerals and indicates that the Luoboling deposit, with uniform molybdenite Re-Os ages of ~105 Ma (Duan et al., 2017; Li and Jiang, 2017; Liang et al., 2012; Zhong et al., 2014), is obviously younger. This observation thus implies that the Luoboling deposit is not the deeper part of the Zijinshan deposit but more likely belongs to another independent hydrothermal system.

5.2. *Distribution trends of trace elements and implications for the origin of fluid*

As described in 'deposit geology', the deep potassic alteration and related porphyry-like Cu-Mo mineralization are generally observed in new deep drill hole DZK707 (< −500 m elevation) in this study (Figs. 3, 4). This zone develops below the phyllic alteration zone and displays the different petrologic, alteration, mineralization characteristics and a large space interval relative to the adjacent Luoboling deposit. The alteration type exhibits a close relationship with trace elements in sulfides, especially pyrite. From the deep potassic zone, the middle phyllic zone to the shallow HS Cu mineralization zone, elements such as Au, As, Ag, Te, Pb and Bi show gradually increasing trends in pyrite, whereas elements such as Co, Ni and Se exhibit inverse decreasing trends (Table 2, Fig. 9). This observation is basically consistent with the results of Franchini et al. (2015) for the typical Agua Rica porphyry-HS epithermal deposit, which indicates that the elements such as Co, Ni and Se are more likely to be concentrated at high-temperature porphyry stage, whereas elements such as Au, As, Ag, Te, Pb and Bi tend to migrate upward and precipitate in epithermal environment at lower temperature. The transitions of mineral associations from Cu-Mo to Cu-Au, alteration types from potassic, phyllic to HSE

Table 3
Summary of dating results for the Zijinshan Cu-Au deposit and the Luoboling Cu-Mo deposit.

Samples	Dating minerals	Dating method	Age (Ma,2σ)	Reference
Zijinshan				
Alteration minerals	Alunite	$^{40}Ar/^{39}Ar$	101.19 ± 0.60~102.86 ± 0.61	Pan et al., 2019
	Muscoveite	$^{40}Ar/^{39}Ar$	113.4 ± 1.1	Huang et al., 2018
	Alunite	K/Ar	103.8	Zhang et al., 1992
	Alunite	K/Ar	111.7	Zhang et al., 1991
	Alunite	K/Ar	89	Zhou and Chen, 1996
	Alunite	K/Ar	82	Zhou and Chen, 1996
	Alunite	K/Ar	101.9 ± 1.3	Zhang et al., 2003
	Quartz	Rb-Sr	122 ± 4	Zhou and Chen, 1996
	Quartz	Rb-Sr	100 ± 3	Zhou and Chen, 1996
Sulfides	Pyrite	Re-Os	103 ± 4	Jiang et al., 2017
	Molybdenite	**Re-Os**	**111.31 ± 0.70**	**This study**
Related volcanic orsubvolcanic rocks	Zircon	LA-ICP-MS U-Pb	104 ± 1~111 ± 0.3	Jiang et al., 2013
	Zircon	LA-ICP-MS U-Pb	107.5 ± 1.4	Duan et al., 2017
	Zircon	LA-ICP-MS U-Pb	104.5 ± 1.6	Duan et al., 2017
	Zircon	LA-ICP-MS U-Pb	105 ± 0.7	Hu et al., 2012
	Zircon	LA-ICP-MS U-Pb	105 ± 2.2	Hu et al., 2012
	Zircon	LA-ICP-MS U-Pb	112.9 ± 1.2	Huang et al., 2018
	Zircon	LA-ICP-MS U-Pb	104.7 ± 0.5	Pan et al., 2019
	Zircon	LA-ICP-MS U-Pb	104.8 ± 0.9	Pan et al., 2019
	Zircon	LA-ICP-MS U-Pb	99.5 ± 0.7	Pan et al., 2019
	Zircon	SHRIMP U-Pb	96 ± 2	Yu et al., 2013
Luoboling				
Sulfides	Molybdenite	Re-Os	105.5 ± 2.2	Duan et al., 2017
	Molybdenite	Re-Os	105.3 ± 1.5	Li and Jiang, 2017
	Molybdenite	Re-Os	104.6 ± 1.0	Zhong et al., 2014
	Molybdenite	Re-Os	104.9 ± 1.6	Liang et al., 2012
Granodiorite porphyry	Zircon	LA-ICP-MS U-Pb	103.8 ± 0.9	Huang et al., 2018
	Zircon	LA-ICP-MS U-Pb	103.7 ± 1.2, 103.0 ± 0.9	Huang et al., 2013
	Zircon	SHRIMP U-Pb	100 ± 2	Yu et al., 2013
	Zircon	LA-ICP-MS U-Pb	98.6 ± 1.2~100.6 ± 1.5	Li et al., 2017
	Zircon	LA-ICP-MS U-Pb	103.1 ± 1.1	Li and Jiang, 2015

alteration, and the behaviors of trace elements in pyrite from different alteration zones at vertical direction reflect a potentially complete transition from porphyry to epithermal mineralization from deep to shallow regions in the Zijinshan deposit. Widespread pyrite-quartz veins in the phyllic zone may play the roles of fluid migration channels.

Regular variations in trace elements with depth have also been recognized, which are mainly reflected in Au and Ag. Samples collected in the HS Cu mineralization zone and HS veins in the phyllic zone present the same mineral association, however, Au exhibits an increasing trend with decreasing depth in pyrite and digenite, and Ag displays similar but more evident variations for bornite, digenite and primary covellite (Fig. 9). These evolution trends can be well explained as that the Au and Ag are transported in upward-migrating fluids that originated from deeper region below the Zijinshan Cu-Au deposit, rather than from the adjacent Luoboling deposit. These trends are consistent with the spatial distributions of alteration and mineralization zones in vertical direction. The increasing precipitation of Au and Ag upward can be attributed to the gradual decreases in temperature and pressure, the progressive fluid-rock interaction or the introduction of meteoric water.

5.3. Implications for Cu-(Fe)-sulfide genesis

The same Cu-(Fe)-sulfides with different genesis usually exhibit different trace element characteristics. As a result, these distribution trends can be used to judge the origin of Cu-(Fe)-sulfides, when geological observations are inoperative.

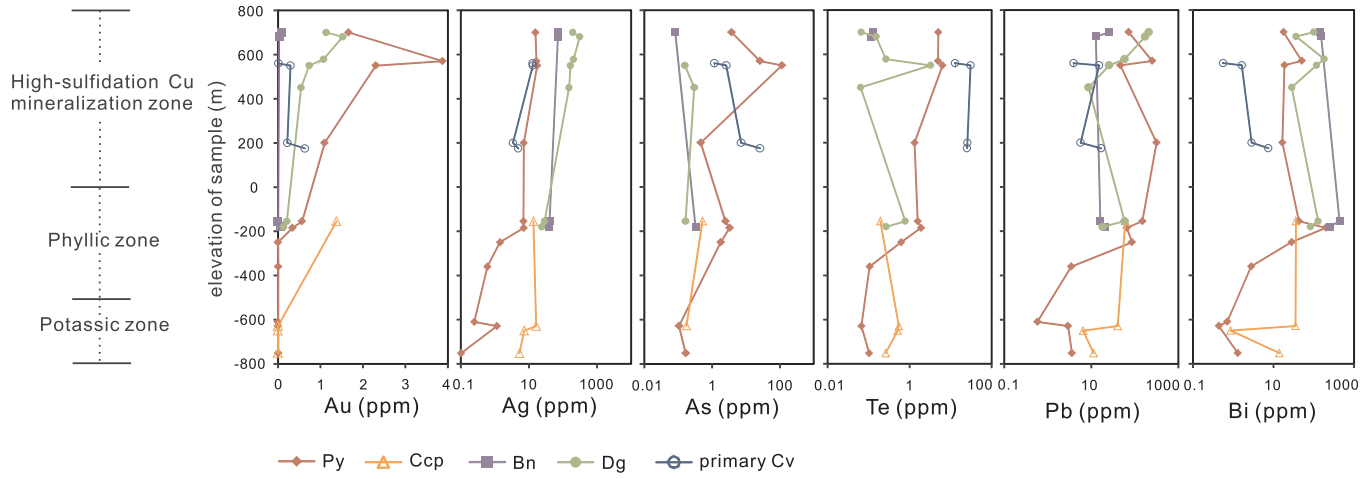

Fig. 9. Distribution of Au, Ag-related trace elements in different sulfide minerals from different alteration types and elevations. *Abbreviations:* Py = pyrite; Ccp = chalcopyrite; Bn = bornite; Dg = digenite; Cv = covellite.

As described above, two different chalcopyrite types have been recognized, one as coarse-grained crystals (Fig. 5a) in quartz-molybdenite-chalcopyrite-pyrite veins of the potassic zone and the other as fine-grained exsolved crystals in bornite or digenite in HS veins of the phyllic zone and the upper HS Cu mineralization zone (Fig. 5e, g. Wu et al., 2017; Zhong et al., 2018; Liu et al., 2016; Cui et al., 2015). These chalcopyrite display completely different trace element characteristics, with the first type enriched in V, Mn, In and Se, whereas the second is enriched in Au and Pb. Undoubtedly, the first type is the product of porphyry-like mineralization stage under high-temperature conditions. However, the particular exsolution texture and trace elements of the second type, especially high Au contents, implying a different genesis. Recently, Li et al. (2018) suggested that the exsolution of this type of chalcopyrite from bornite-digenite solid solutions is the product of 'back-reaction', which occurred during low-temperature annealing (150°C). The chalcopyrite in the HS zone possibly has a similar genesis and the distinctive high content of Au is the heritage from earlier bornite-digenite solid solutions.

Zhong et al. (2018) proposed that chalcopyrite and bornite in the HS Cu mineralization zone of the Zijinshan deposit are the products of earlier overprinted porphyry mineralization. As discussed above, chalcopyrite in the HS ores is more likely result from 'back-reaction' at epithermal stage. Cook et al. (2011) studied trace elements of bornite in different deposit types, showing the trend of decreasing Bi and Ag contents with decreasing mineralization temperature. In addition, when bornite and digenite coexist, silver preferentially enters digenite, whereas Bi tends to be incorporated in bornite. Compared with the data from Cook et al. (2011), bornite in the Zijinshan deposit carries the least Ag and Bi (Fig. 10a), suggest epithermal genesis at low temperature. Samples with coexisting bornite and digenite in HS Cu zone display a good trend that Bi entering bornite and Ag entering digenite (Fig. 10b), indicating the element equilibrium between digenite and bornite. Thus, similar to chalcopyrite, bornite is also the product of the epithermal stage that is synchronous with digenite, rather than a residue of earlier porphyry mineralization.

Digenite and covellite are the two most important Cu-carrying minerals in Zijinshan, and their genesis is still debatable. Ruan et al. (2009) proposed that digenite and covellite partly formed through secondary enrichment involving dissolution of primary Cu ores by acidic fluids. However, most authors argued for a primary hydrothermal genesis based on mineralogy, ore structure and Cu isotopes (Qiu et al., 2010; Lin, 2012; Wu et al., 2017). Reich et al. (2010) reported trace elements of supergene digenite from various Cu deposits in northern Chile, which show distinctly higher contents of Au, Ag, As, Sb and Te than the Zijinshan deposit. In addition, the recognized intimate relationship among Au, Ag and As in Chile is also absent in this study as a result of very low contents of As. Contents of As that are generally below the mdl also appears in primary digenite reported by Cook et al. (2011). Similarly, Sb is also absent in Cook et al. (2011) and in our study but enriched in supergene digenite. Entirely different trace elements, especially indicative As and Sb, as well as the absence of most trace elements except exclusive Au, Ag, Pb and Bi indicate that the digenite of the Zijinshan deposit has a primary hydrothermal genesis.

Only one possible supergene covellite sample at the top (+700 m elevation) is distinguished from other dominant primary covellite samples in the deeper part of the ore body based on the mineralogical features (Figs. 4c; 5l). Trace elements in these two different types of covellite exhibit a large gap (Table 2), which is characterized by dramatic increases in most elements (such as W, Sb, As, Au, Ag and Pb) and decreases in Se and Te in supergene covellite. In fact, secondary enrichments in Au and Ag of Cu-sulfides have already been recognized (Hannington et al., 1988; Mozgova et al., 2008; Reich et al., 2010). Melekestseva et al. (2017) reported trace elements in secondary covellite from the Semenov-2 hydrothermal field, which also displays 1–3 orders of magnitude higher contents of As, Ag, Sb, Au and Pb compared with primary sulfides, consistent with the trend at Zijinshan. Combining

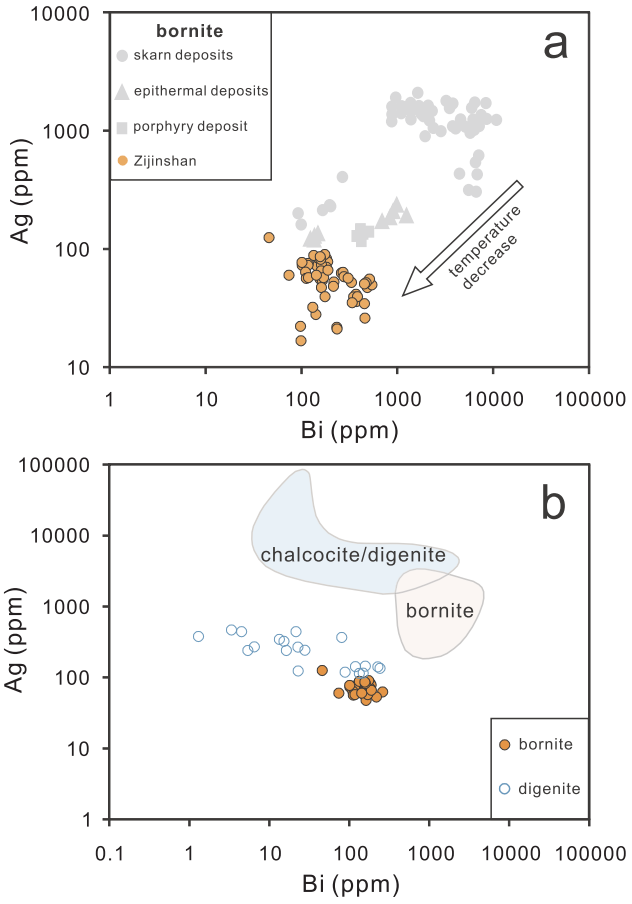

Fig. 10. Log-log plot of Bi vs. Ag concentrations in (a) bornite and (b) bornite and digenite. Bornite from the Zijinshan deposit hosts the least Bi and Ag compared with other deposits reported by Cook et al (2011) (gray data plots) in diagram a, indicating low-temperature genesis. The trend of Bi entering bornite and Ag entering digenite is obvious in samples from HSE Cu mineralization zone in diagram b, similar to that recognized by Cook et al (2011) (light blue and yellow area), indicating the syncrystallization of bornite and digenite. (For interpretation of the references to colour in this figure legend, the reader is referred to the web version of this article.)

mineralogy and trace element characteristics, hypogene covellite is also dominant in the Zijinshan deposit, whereas minor supergene covellite may also occur at the top of the Cu ore body that is close to the oxidation and leaching zone. The supergene process will cause the dramatic enrichment of most trace elements in sulfides, especially Ag.

5.4. Enrichments of Au and Ag

Pyrite and digenite formed in the HS stage in this study are two major sulfides that carry primary Au based on Au concentrations and amounts of corresponding minerals. The enrichment of Au in digenite is also reported by Liu et al. (2017). Recently, Liu et al. (2019) reported enrichment of Au in enargite. In contrast, bornite and digenite are good carriers of primary Ag. In correlation diagrams, no evident relationship can be observed between Au and As in pyrite (Fig. 11a). Spots with As contents higher than 5 ppm are generally influenced by enargite and As-bearing secondary covellite inclusions, whereas pure pyrite displays As concentrations only below or around the detection limits. In addition, inconsistent behaviors of Au and As in depth profiles indicate that As is not the key element promoting Au to enter pyrite as observed in other Au deposits (e.g., Cline, 2001; Reich et al., 2005, 2013; Muntean et al., 2011; Deditius et al., 2008; Large et al., 2007; Morey et al., 2008; Foster et al., 2007). In contrast, Au exhibits good correlation with Te

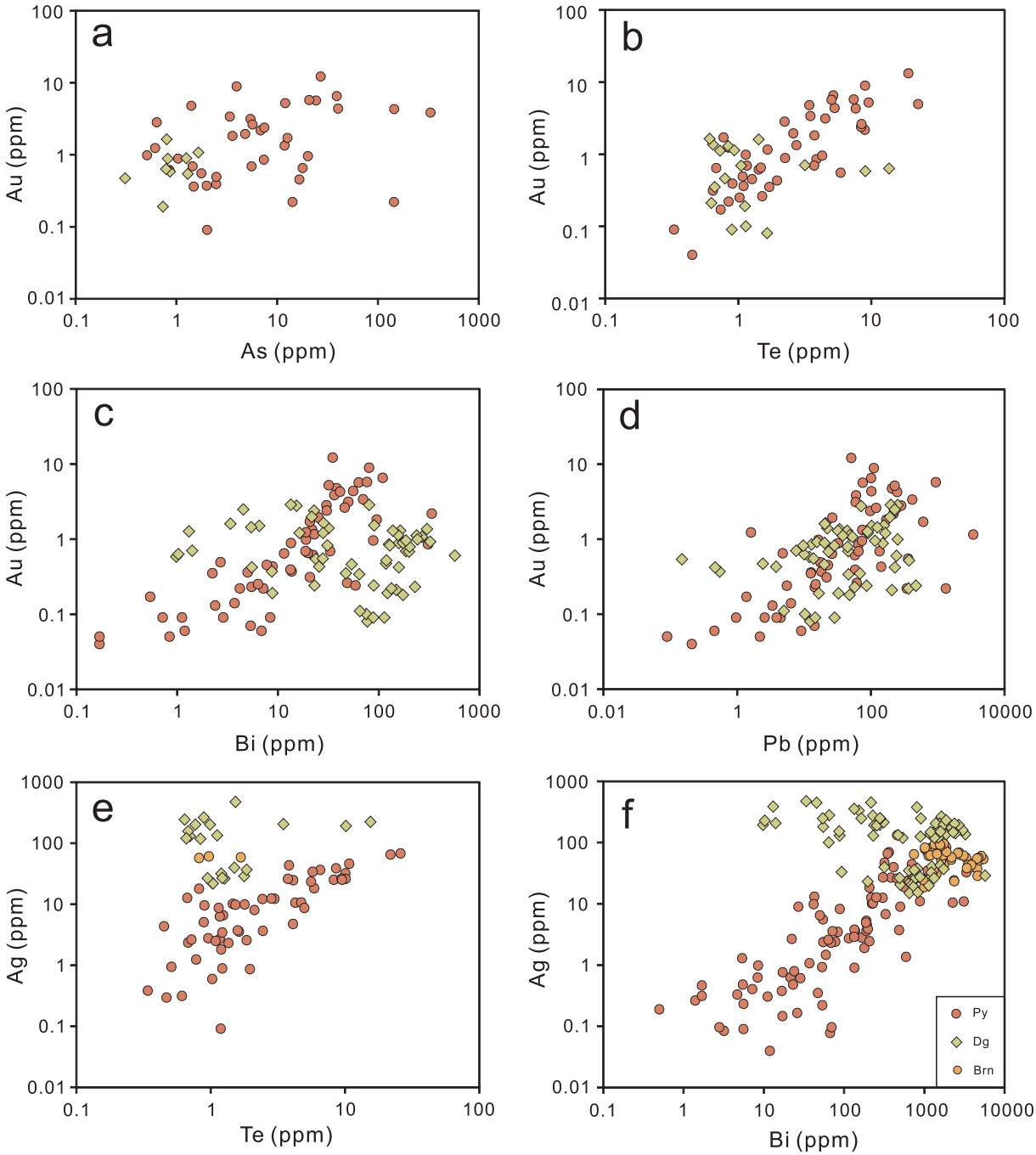

Fig. 11. Correlation diagrams of different elements vs. Au and Ag concentrations in pyrite, digenite, and bornite (complete dataset). a. Au-As; b. Au-Te; c. Au-Bi; d. Au-Pb; e. Ag-Te; f. Ag-Bi. *Abbreviations:* Py = pyrite; Dg = digenite; Bn = bornite.

and common correlations with Bi and Pb (Fig. 11b, c, d), whereas Ag displays good correlation with Te and Bi (Fig. 11e, f). Intimate relationships between Au and Te have also been discovered in other As-free Au deposits (e.g., Pals et al., 2003; Sung et al., 2009; Cook et al., 2009; Bi et al., 2011; Ciobanu et al., 2010, 2012) and in enargite at Zijinshan (Liu et al., 2019). Bi is also recently discovered to significant for Au enrichment in porphyry system (Zhou et al., 2016, 2017). Te and Bi as part of the low melting point chalcophile group elements (LMCE; Frost et al., 2002; Cook et al., 2009), have been proposed to assist incorporation of Au within melts, without requiring fluid saturation with respect to a Au mineral (e.g., Ciobanu et al., 2005, 2006; Cook et al., 2009; Tooth et al., 2011). These two elements are thus thought to be significant for scavenging Au into pyrite from fluids to achieve primary stage Au enrichment at Zijinshan. In fact, the good correlations between Te, Bi and Ag, also imply similar situations. Liu et al. (2015, 2017) suggested that primary gold in the Zijinshan deposit mainly occurs as native particles or Te-Au compounds. No independent primary native Au and Ag minerals were observed in our study. According to the LA-ICP-MS depth profiles (Fig. 8) and BSE observations (Fig. 12), Te, Au and Ag are mainly together locked in pyrite lattice (or exist as Te-Au-Ag nanoparticles), locally form visible Au-Ag-telluride (Fig. 12a), although the specific substitution mechanism is still unclear (Bi et al., 2011; Cook et al., 2009). Bi, Pb, Au and Ag are also usually together locked in lattice (or exist as nanoparticles) but constitute more abundant micron to submicron Bi-sulfosalt inclusions in pyrite, which are usually observed in depth profiles and BSE images (Figs. 8a; 12b).

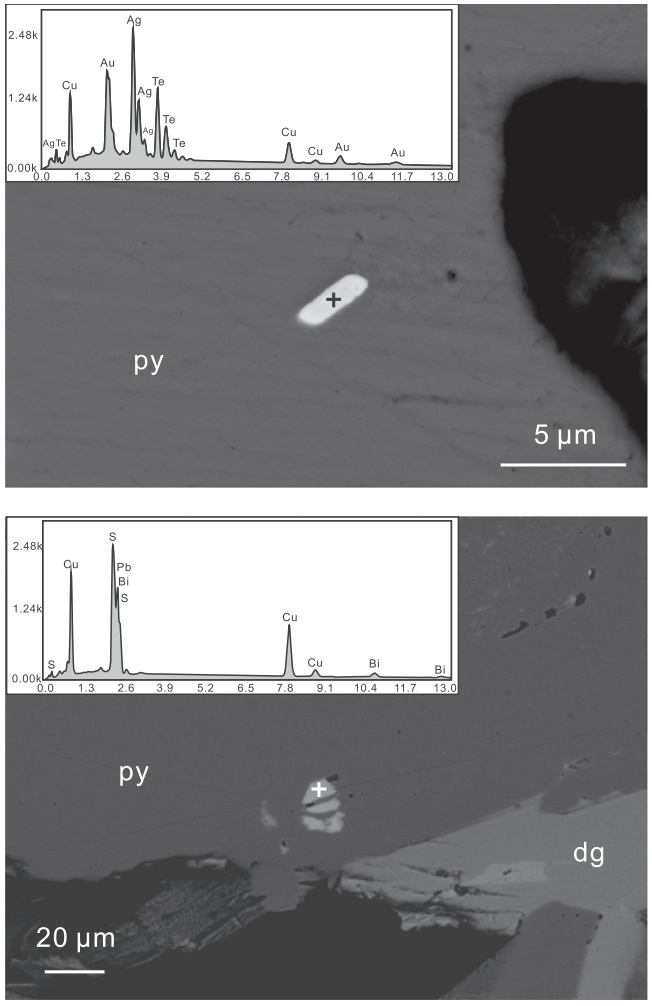

Fig. 12. BSE image and corresponding energy dispersive spectrometry (EDS) spectrum of (a) Au-Ag-telluride and (b) Bi-sulfosalt in pyrite from the HS Cu mineralization zone. *Abbreviations:* Py = pyrite. Dg = digenite.

Digenite is another carrier of primary Au and the most significant sulfide to carry primary Ag. Au and Ag in digenite always display consistent contents (in same samples), smooth profiles (Fig. 8d) and show no correlations with other elements such as Te, Bi and Pb (Fig. 11), suggesting that the Au and Ag are not hosted by other mineral phases such as telluride and Bi-sulfosalt inclusions, but is mainly locked in the digenite structure or occurs as native nanoparticles. The entire absence of correlations between Au and the elements As, Te, Bi and Pb also imply the different mechanism of Au enrichment in digenite from pyrite. Au and Ag more likely independently enter the digenite lattice as isomorphism form to substitute Cu under an equilibrium environment, rather than attracted by Bi and Te. Bornite as another major sulfide to host Ag also displays similar characteristics.

Based on mineralogical observations, the four Cu-(Fe)-sulfides analyzed in this study constitute a major paragenetic sequence of chalcopyrite → bornite → digenite → covellite (Liu et al., 2016; Cui et al., 2015). This mineral sequence is controlled by a complete evolution of the sulfidation state from the 'intermediate' to the 'very high' condition (Fig. 13), as a result of an increase in sulfur fugacity or a decrease in temperature (Einaudi et al., 2003). The enrichments of Au and Ag in digenite indicate that the primary precipitation of Au and Ag mainly occurred during the high sulfidation state stage (Fig. 13). Large amounts of Au and Ag precipitated with digenite, pyrite and enargite (Liu et al., 2019), thereafter causing the deficit of Au and Ag in covellite at the very high sulfidation state stage. The upward increasing

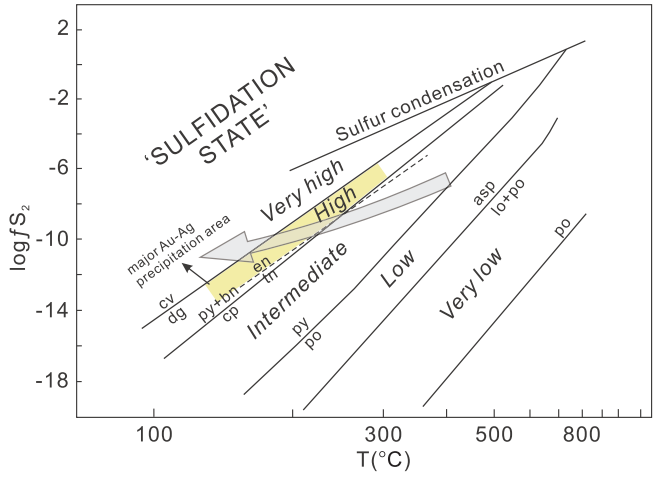

Fig. 13. Bivariate plot of logfS_2 vs. temperature reflecting the variation of sulfidation state (after Einaudi et al., 2003). The gray arrow displays a possible evolution path of sulfidation state from intermediate to very high at Zijinshan, based on paragenetic sequence of major Cu-(Fe)-sulfide minerals. The temperature range is based on the microthermetric results of fluid inclusion from So et al. (1998) and Zhong et al. (2018). The yellow area represents the possible major region for Au-Ag precipitation. (For interpretation of the references to colour in this figure legend, the reader is referred to the web version of this article.)

concentrations of Au and Ag in respective sulfides from the primary HS Cu zone result in the first (primary) stage enrichment of Au at the top. However, the generally low absolute Au concentrations in primary sulfides are far from enough to provide ~305 t Au reserves, although the later leaching and oxidation process (secondary enrichment) occurred. This deficit indicate the potential existence of a more enriched primary Au ore body at the top to provide sufficient Au, which however, has not been preserved. The supergene process caused the second-stage enrichment in Au and Ag. Leaching and oxidation processes controlled by later multistage faults resulted in the loss of Cu and further concentration of Au at the top (Cui et al., 2015; Liu et al., 2017; Jiang et al., 2017). This process can be indentified by the strict confinement of the Au ore body in the oxidation-leaching zone and enrichments of Au and Ag in secondary covellite, limonite and goethite. Supergene and hypogene processes together caused the enrichment of ore-forming metals and the mineralization pattern of dominant Au in the upper part and major Cu in the lower part of the deposit.

Regular variations of Au and Ag increasing upward within the primary Cu mineralization zone, the occurrence of deep potassic alteration with Cu-Mo mineralization, as well as the molybdenite Re-Os age, indicate that the ore-forming fluids of the Zijinshan deposit most likely originate from the deep region, rather than from the adjacent Luoboling deposit. The Zijinshan and the Luoboling deposits should belong to two independent hydrothermal systems.

6. Conclusions

1. Molybdenite Re-Os dating yields weighted average age of 111.31 ± 0.70 Ma, implying the initiation of Cu-Au mineralization at Zijinshan. This result is obviously older than the adjacent Luoboling porphyry Cu-Mo deposit with a Re-Os age of ~105 Ma.
2. The spatial zonings of mineralization (from Cu-Mo to Cu-Au), alteration (from potassic, phyllic to HSE alterations), and the regular variations of trace elements in sulfides vertically imply a complete transition from porphyry to epithermal mineralization and the deep origin of ore-forming fluids.
3. Based on trace elemental and mineralogical observations, bornite and fine-grained chalcopyrite developed in the HS Cu zone are products of epithermal mineralization stage at low temperature,

rather than residues of overprinted porphyry mineralization as reported previously. The majority of digenite and covellite have hypogene genesis.

4. Pyrite and digenite in the HSE zone are major carriers of primary Au. Au in pyrite is obviously Te-Bi related and exists as solid solutions or different-sized telluride and Bi-sulfosalt inclusions. Au in digenite independently exists as solid solution. Bornite and digenite are good carriers of primary Ag. The high sulfidation state stage is the major period for concentrations of primary Au and Ag. Hypogene and supergene processes together produce the distribution pattern of upper Au enrichment and lower Cu enrichment.
5. Based on the alteration and mineralization zonings, the spatial variation of trace elements and the presented Re-Os age, the Zijinshan deposit most likely belong to an independent hydrothermal system that originated from deep region, rather than from the adjacent Luoboling porphyry deposit.

Declaration of Competing Interest

The authors declare that they have no known competing financial interests or personal relationships that could have appeared to influence the work reported in this paper.

Acknowledgments

This paper is financially supported by the National Key R&D Program of China (2016YFC0600405) and the National Natural Science Foundation of China (Grant No. 41425011 and 41703049). The field work is strongly supported by the Zijin Mining Co. Ltd. We thank two anonymous reviewers for their constructive comments. We also appreciate the assistance of Drs. Li Chao and Dai Zhihui for the lab works.

Appendix A. Supplementary data

Supplementary data to this article can be found online at https://doi.org/10.1016/j.oregeorev.2020.103363.

References

Bi, S.J., Li, J.W., Zhou, M.F., Li, Z.K., 2011. Gold distribution in As-deficient pyrite and telluride mineralogy of the Yangzhaiyu gold deposit, Xiaoqinling district, southern North China craton. Miner. Deposita 46, 925–941.

Chen, H.S., 1996. The research on the mineralization chronology and isotopic exploration assessment for Zijinshan copper-gold deposit. Geotecton. Metallog. 20, 348–360 (in Chinese with English abstract).

Chen, J., Chen, Y.J., Zhong, J., Sun, Y., Li, J., Qi, J.P., 2011. Fluid inclusion study of the Wuziqilong Cu deposit in the Zijinshan ore field, Fujian Province. Acta Petrol. Sin. 27, 1425–1438 (in Chinese with English abstract).

Chen, J., Chen, Y.J., Zhong, J., Sun, Y., Qi, J.P., Li, J., 2015. Geological and ore-fluid characteristics of Longjiangting Cu deposit in Zijinshan Orefield, Fujian Province, and their genetic implications. Miner. Deposits 34, 98–118 (in Chinese with English abstract).

Chen, J., Cooke, D.R., Piquer, J., Selley, D., Zhang, L., White, N.C., 2019. Hydrothermal alteration, mineralization, and structural geology of the Zijinshan high-sulfidation Au-Cu deposit, Fujian Province, Southeast China. Econ. Geol. 114, 639–666.

Ciobanu, C.L., Cook, N.J., Pring, A., 2005. Bismuth tellurides as gold scavengers. In: Mao, J.W., Mao, F.P., Bierlein (Eds.), Mineral Deposit Research: Meeting the Global Challenge. Springer Berlin-Heidelberg, New York, pp. 1383–1386.

Ciobanu, C.L., Cook, N.J., Damian, F., Damian, G., 2006. Gold scavenged by bismuth melts: an example from Alpine shear-remobilisates in the Highiş Massif, Romania. Mineral. Petrol. 87, 351–384.

Ciobanu, C.L., Birch, W.D., Cook, N.J., Pring, A., Grundler, P.V., 2010. Petrogenetic significance of Au-Bi-Te-S associations: the example of Maldon, Central Victorian gold province, Australia. Lithos 11, 1–17.

Ciobanu, C.L., Cook, N.J., Utsunomiya, S., Kogagwa, M., Green, L., Gilbert, S., Wade, B., 2012. Gold-telluride nanoparticles revealed in arsenic-free pyrite. Am. Mineral. 97, 1515–1518.

Cline, J.S., 2001. Timing of gold and arsenic sulfide mineral deposition at the Getchell Carlin-type gold deposit, North-Central Nevada. Econ. Geol. 96, 75–89.

Cook, N.J., Ciobanu, C.L., Mao, J.W., 2009. Textural control on gold distribution in As-free pyrite from the Dongping, Huangtuliang and Hougou gold deposits, North China Craton (Hebei Province, China). Chem. Geol. 264, 101–121.

Cook, N.J., Ciobanu, C.L., Danyushevsky, L.V., Gilbert, S., 2011. Minor and trace elements in bornite and associated Cu–(Fe)–sulfides: a LA-ICP-MS study. Geochim. Cosmochim. Acta 75, 6473–6496.

Cook, N.J., Ciobanu, C.L., Meria, D., Silcock, D., Wade, B., 2013. Arsenopyrite-pyrite association in an orogenic gold ore: tracing mineralization history from textures and trace elements. Econ. Geol. 108, 1273–1283.

Cui, X.L., Liu, W.Y., Liu, Y., Li, X.M., 2015. Research progress on ore geology of Zijinshan high- sulphidation Au–Cu deposit. Acta Mineral Sin. 35, 167–177 (in Chinese with English abstract).

Danyushevsky, L.V., Robinson, P., Gilbert, S., Norman, M., Large, R., McGoldrick, P., Shelley, J.M.G., 2011. Routine quantitative multi-element analysis of sulphide minerals by laser ablation ICP-MS: standard development and consideration of matrix effects. Geochem. Explor. Environ. Anal. 11, 51–60.

Deditius, A.P., Utsunomiya, S., Renock, D., Ewing, R.C., Ramana, C.V., Becker, U., Kesler, S.E., 2008. A proposed new type of arsenian pyrite: composition, nanostructure and geological significance. Geochim. Cosmochim. Acta 72, 2919–2933.

Deditius, A.P., Reich, M., Kesler, S.E., Utsunomiya, S., Chryssoulis, S.L., Walshe, J., Ewing, R.C., 2014. The coupled geochemistry of Au and As in pyrite from hydrothermal ore deposits. Geochim. Cosmochim. Acta 140, 644–670.

Du, A.D., He, H.L., Yin, W.N., 1994. A study on the rhenium–osmium geochronometry of molybdenites. Acta. Geol. Sin. 68, 339–347 (in Chinese with English abstract).

Du, A.D., Wu, S.Q., Sun, D.Z., Wang, S.X., Qu, W.Q., Markey, R., Stain, H., Morgan, J., Malinovskiy, D., 2004. Preparation and certification of Re/Os dating reference materials: molybdenites HLP and JDC. Geostand. Geoanal. Res. 28, 41–52.

Duan, G., Chen, H., Hollings, P., Qi, J., Xu, C., Zhang, S., Xiao, B., Liu, G.Y., Liu, J., 2017. The Mesozoic magmatic sources and tectonic setting of the Zijinshan mineral field, South China: constraints from geochronology and geochemistry of igneous rocks in the Southeastern ore segment. Ore Geol. Rev. 80, 800–827.

Einaudi, M.T., Hedenquist, J.W., Inan, E.E., 2003. Sulfidation state of fluids in active and extinct hydrothermal systems: transitions from porphyry to epithermal environments. Soc. Econ. Geol. Spec. Publ. 10, 285–313.

Foster, A.R., Williams, P.J., Ryan, C.G., 2007. Distribution of gold in hypogene ore at the Ernest Henry iron oxide copper-gold deposit, Cloncurry District, NW Queensland. Explor. Min. Geol. 16, 125–143.

Franchini, M., McFarlane, C., Maydagán, L., Reich, M., Lentz, D.R., Meinert, L., Bouhier, V., 2015. Trace metals in pyrite and marcasite from the Agua Rica porphyry-high sulfidation epithermal deposit, Catamarca, Argentina: textural features and metal zoning at the porphyry to epithermal transition. Ore Geol. Rev. 66, 366–387.

Frost, B.R., Mavrogenes, J.A., Tomkins, A.G., 2002. Partial melting of sulfide ore during medium- and high-grade metamorphism. Can. Mineral. 40, 1–18.

Hannington, M.D., Thompson, G., Rona, P.A., Scott, S.D., 1988. Gold and native copper in supergene sulfides from the Mid-Atlantic Ridge. Nature 333, 64–66.

Hedenquist, J.W., Arribas Jr., A., Reynolds, T.J., 1998. Evolution of an intrusion-centered hydrothermal system: far Southeast-Lepanto porphyry and epithermal Cu-Au deposits, Philippines. Econ. Geol. 93, 373–404.

Hedenquist, J.W., Arribas, A., Jr., Gonzalez-Urien, E., 2000. Exploration for epithermal gold deposits: Reviews in Econ. Geol. 13, 245 – 277.

Heinrich, C.A., Driesner, T., Stefánsson, A., Seward, T.M., 2004. Magmatic vapor contraction and the transport of gold from the porphyry environment to epithermal ore deposits. Geology 32, 761–764.

Heinrich, C.A., 2005. The physical and chemical evolution of low-salinity magmatic fluids at the porphyry to epithermal transition: a thermodynamic study. Miner. Deposita 39, 864–889.

Hu, C.J., Huang, W.T., Bao, Z.W., Liang, H.Y., Wang, C.L., 2012. LA-ICP-MS zircon U-Pb dating of the dacite porphyry from Zijinshan Cu-Au deposit and its metallogenic implications. Geotecton. Metallog. 36, 284–292 (in Chinese with English abstract).

Huang, W.T., Liang, H.Y., Wu, L., Wu, J., Li, J., Bao, Z.W., 2018. Asynchronous formation of the adjacent epithermal Au-Cu and porphyry Cu-Mo deposits in the Zijinshan orefield, southeast China. Ore Geol. Rev. 102, 351–367.

Huang, W.T., Li, J., Liang, H.Y., Wang, C.L., Lin, S.P., Wang, X.Z., 2013. Zircon LA-ICP-MS U-Pb ages and highly oxidized features of magma associated with Luoboling porphyry Cu-Mo deposit in Zijinshan ore field, Fujian Province. Acta. Petrol. Sin. 29, 283–293 (in Chinese with English abstract).

Jiang, S.H., Bagas, L., Liang, Q.L., 2015. New insights into the petrogenesis of volcanic rocks in the Shanghang Basin in the Fujian Province, China. J. Asian. Earth Sci. 105, 48–67.

Jiang, S.H., Bagas, L., Liang, Q.L., 2017. Pyrite Re-Os isotope systematics at the Zijinshan deposit of SW Fujian, China: constraints on the timing and source of Cu-Au mineralization. Ore Geol. Rev. 80, 612–622.

Jiang, S.H., Liang, Q.L., Bagas, L., Wang, S.H., Nie, F.J., Liu, Y.F., 2013. Geodynamic setting of the Zijinshan porphyry-epithermal Cu–Au–Mo–Ag ore system, SW Fujian Province, China: constrains from the geochronology and geochemistry of the igneous rocks. Ore Geol. Rev. 53, 287–305.

Large, R.R., Maslennikov, V.V., Robert, F., Danyushevsky, L., Chang, Z., 2007. Multistage Sedimentary and metamorphic origin of pyrite and gold in the giant Sukhoi Log deposit, Lena gold province, Russia. Econ. Geol. 102, 1233–1267.

Li, B., Jiang, S.Y., 2015. A subduction-related metasomatically enriched mantle origin for the Luoboling and Zhongliao Cretaceous granitoids from the Zijinshan ore district of Fujian Province in South China: implications for magma evolution and Cu–Mo mineralization. Int. Geol. Rev. 57, 1239–1266.

Li, B., Jiang, S.Y., 2017. Genesis of the giant Zijinshan epithermal Cu-Au and Luoboling porphyry Cu–Mo deposits in the Zijinshan ore district, Fujian Province, SE China: a multi-isotope and trace element investigation. Ore Geol. Rev. 88, 753–767.

Li, B., Jiang, S.Y., Lu, A.H., Zhao, H.X., Yang, T.L., Hou, M.L., 2016. Zircon U-Pb dating, geochemical and Sr–Nd–Hf isotopic characteristics of the Jintonghu monzonitic rocks in western Fujian Province, South China: implication for Cretaceous crust–mantle interactions and lithospheric extension. Lithos 260, 413–428.

Li, B., Zhao, K.D., Yang, S.Y., Dai, B.Z., 2013. Petrogenesis of the porphyritic dacite from

Ermiaogou Cu–Au deposit in Zijinshan ore field and its metallogenetic implications. Acta. Petrol. Sin. 29, 4167–4185 (in Chinese with English abstract).
Li, K., Brugger, J.L., Pring, A., 2018. Exsolution of chalcopyrite from bornite-digenite solid solution: an example of a fluid-driven back-replacement reaction. Miner. Deposita 53, 903–908.
Li, C.Y., Hao, X.L., Liu, J.Q., Ling, M.X., Ding, X., Zhang, H., Sun, W.D., 2017. The formation of Luoboling porphyry Cu-Mo deposit: constraints from zircon and apatite. Lithos 272–273, 291–300.
Liang, Q.L., Jiang, S.H., Wang, S.H., Li, C., Zeng, F.G., 2012. Re-Os Dating of molybdenite from the luoboling porphyry Cu-Mo deposit in the Zijinshan ore field of Fujian Province and its geological significance. Acta. Geol. Sin. 86, 1113–1118 (in Chinese with English abstract).
Liang, Q.L., Jiang, S.H., Wang, S.H., Liu, Y.F., Bai, D.M., Chen, C.L., 2013. Petrogenesis of the Mesozoic magmatic rocks in Zijinshan area: constraints from zircon Hf isotope evidence. Acta. Petrol. Mineral. 32, 318–328 (in Chinese with English abstract).
Lin, Y.X., 2012. Elementary introduction to characteristics of digenite and other sulfides in Zijinshan copper mining district. Contrib. Geol. Mineral. Resour. Res. 27, 66–70 (in Chinese with English abstract).
Liu, W.Y., 2015. Mineralogy of the Zijinshan Porphyry-epithermal system, Fujian Province. Dissertation. Chinese Academy of Geological Sciences.
Liu, W.Y., Cook, N.J., Ciobanu, C.L., Gilbert, S.E., 2019. Trace element substitution and grain-scale compositional heterogeneity in enargite. Ore Geol. Rev. 111, 103004.
Liu, W.Y., Chen, Y.C., Liu, Y., 2017. EPMA and LA-ICP-MS microanalysis of Cu-Fe-S minerals in Zijinshan orefield: implications for ore genesis. Earth Sci. Front. 24, 39–53 (in Chinese with English abstract).
Liu, W.Y., Cook, N.J., Ciobanu, C.L., Liu, Y., Qiu, X.P., Chen, Y.C., 2016. Mineralogy of tin-sulfides in the Zijinshan porphyry-epithermal system, Fujian Province. China. Ore Geol. Rev. 72, 682–698.
Mao, J.R., Tao, K.Y., Lee, J.Y., Xie, F.G., Xu, N.Z., 2002. Geochronology and geochemical characteristics in late Mesozoic Sifang pluton, southwestern Fujian, and their significanc. Acta. Petrol. Sin. 18, 449–458 (in Chinese with English abstract).
Mao, J.W., Cheng, Y.B., Chen, M.H., Pirajno, F., 2013. Major types and time–space distribution of Mesozoic ore deposits in South China and their geodynamic settings. Miner. Deposita 48, 267–294.
Melekestseva, I.Y., Maslennikov, V.V., Maslennikova, S.P., Danyushevsky, L.V., Large, R., 2017. Covellite of the Semenov-2 hydrothermal field (13° 31.13′ N, Mid-Atlantic Ridge): enrichment in trace elements according to LA ICP MS analysis. Dokl. Earth Sci. 473, 291–295.
Morey, A.A., Tomkins, A.G., Bierlin, F.P., Wienberg, R.F., Davidson, G.J., 2008. Bimodal distribution of gold in pyrite and arsenopyrite: examples from the Archean Boorara and Bardoc shear systems, Yilgarn craton, Western Australia. Econ. Geol. 103, 599–614.
Mozgova, N.N., Trubkin, N.V., Borodaev, Y.S., Cherkashev, G.A., Stepanova, T.V., Semkova, T.A., Upenskaya, T.Y., 2008. Mineralogy of massive sulfides from the Ashadze hydrothermal field, 13_N, Mid-Atlantic Ridge. Can. Mineral. 46, 545–567.
Muntean, J.L., Cline, J.S., Simon, A.C., Longo, A.A., 2011. Magmatic-hydrothermal origin of Nevada's Carlin-type gold deposits. Nature Geosci. 4, 122–127.
Pals, D.W., Spry, P.G., Chryssoulis, S., 2003. Invisible gold and tellurium in arsenic-rich pyrite from the Emperor gold deposit, Fiji: implications for gold distribution and deposition. Econ. Geol. 98, 479–493.
Pan, J.Y., Ni, P., Chi, Z., Wang, W.B., Zeng, W.C., Xue, K., 2019. Alunite 40Ar/39Ar and Zircon U-Pb constraints on the magmatic-hydrothermal history of the Zijinshan high-sulfidation epithermal Cu-Au deposit and the adjacent luoboling porphyry Cu-Mo deposit, South China: implications for their genetic association. Econ. Geol. 114, 667–695.
Piquer, J., Cooke, D.R., Chen, J., Zhang, L., 2017. Synextensional emplacement of porphyry Cu-Mo and epithermal mineralization: the Zijinshan District, Southeastern China. Econ. Geol. 112, 1055–1074.
Qiu, X.P., Lan, Y.Z., Liu, Y., 2010. The key to the study of deep mineralization and the evalution of ore-prospecting potential in the Zijinshan gold and copper deposit. Acta. Geosci. Sin. 31, 209–215 (in Chinese with English abstract).
Reich, M., Chryssoulis, S.L., Deditius, A., Palacios, C., Zuniga, A., Weldt, M., Alvear, M., 2010. "Invisible" silver and gold in supergene digenite ($Cu_{1.8}S$). Geochim. Cosmochim. Acta 74, 6157–6173.
Reich, M., Deditius, A., Chryssoulis, S., Li, J.W., Ma, C.Q., Parada, M.A., Barra, F., Mittermayr, F., 2013. Pyrite as a record of hydrothermal fluid evolution in a porphyry copper system: A SIMS/EMPA trace element study. Geochim. Cosmochim. Acta 104, 42–62.
Reich, M., Kesler, S.E., Utsunomiya, S., Palenik, C.S., Chryssoulis, S.L., Ewing, R.C., 2005. Solubility of gold in arsenian pyrite. Geochim. Cosmochim. Acta 69, 2781–2796.
Ruan, S.K., Gong, J.S., Li, W., Dong, Y.X., 2009. Geological characteristics and genesis of Wuziqilong copper deposits in Zijinshan area. Nonferrous Metals 61, 37–42 (in Chinese with English abstract).
Sillitoe, R.H., 2010. Porphyry copper systems. Econ. Geol. 105, 3–41.
Smoliar, M.I., Walker, R.J., Morgan, J.W., 1996. Re-Os ages of group IIA, IIIA, IVA, and IVB iron meteorites. Science 271, 1099–1102.
So, C.S., Zhang, D.Q., Yun, S.T., Li, D.X., 1998. Alteration-mineralization zoning and fluid inclusions of the high sulfidation epithermal Cu–Au mineralization at Zijinshan, Fujian Province, China. Econ. Geol. 93, 961–980.
Sung, Y.H., Brugger, J., Ciobanu, L., Pring, A., Skinner, W., Nugus, M., 2009. Invisible gold in arsenian pyrite and arsenopyrite from a multistage Archaean gold deposit: Sunrise Dam, Eastern Goldfields Province, Western Australia. Miner. Deposita 44, 765–791.
Tooth, B., Ciobanu, C.L., Green, L., O'Neill, B., Brugger, J., 2011. Bi-melt formation and gold scavenging from hydrothermal fluids: an experimental study. Geochim. Cosmochim. Acta 75, 5423–5443.
Wang, C.Z., Jue, H.H., 2013. Mineralogical characteristics of alunite from Zijinshan gold-copper deposit. Acta. Mineral. Sin. 33, 329–336 (in Chinese with English abstract).
Wang, S.H., Pei, R.F., Zeng, X.H., Qiu, X.P., Wei, M., 2009. Metallogenic series and model of the Zijinshan Mining Field. Acta Geol. Sin. 83, 146–157.
Wilson, S.A., Ridley, W.I., Koenig, A.E., 2002. Development of sulfide calibration standards for the laser ablation inductively-coupled plasma mass spectrometry technique. J. Anal. At. Spectrom. 17, 406–409.
Wu, L.Y., Hu, R.Z., Li, X.F., Liu, S.A., Tang, Y.W., Tang, Y.Y., 2017. Copper isotopic compositions of the Zijinshan high-sulfidation epithermal Cu–Au deposit, South China: implications for deposit origin. Ore Geol. Rev. 83, 191–199.
Wu, L.Y., Hu, R.Z., Li, X.F., Stuart, F.M., Jiang, G.H., Qi, Y.Q., Zhu, J.J., 2018. Mantle volatiles and heat contributions in high sulfidation epithermal deposit from the Zijinshan Cu-Au-Mo-Ag orefield, Fujian Province, China: evidence from He and Ar isotopes. Chem. Geol. 480, 58–65.
Xu, C., Chen, H.Y., Huang, W., Qi, J., Duan, G., Zhang, L.J., Wu, C., Zhang, S., Zhong, W.B., 2016. Mesozoic multiphase magmatism at the Xinan Cu–Mo ore deposit (Zijinshan Orefield): geodynamic setting and metallogenic implications. Ore Geol. Rev. 88, 768–790.
Xue, K., Ni, S.K., 2008. Geological characteristics and genesis of the Luobuling copper (Molybdenum) deposit in Zijinshan Orefield. Fujian. Resour. Environ. Eng. 22, 491–496 (in Chinese with English abstract).
Yu, B., Pei, R.F., Qiu, X.P., Chen, J.H., Li, D.P., Zhang, W.H., Liu, W.Y., 2013. The evolution series of mesozoic magmatic rocks in the Zijinshan orefield, Fujian Province. Acta Geol. Sin. 34, 437–446 (in Chinese with English abstract).
Zhang, D.Q., Feng, C.Y., Li, D.X., She, H.Q., Dong, Y.J., 2005. The evolution of ore forming fluids in the porphyry-epithermal metallogenic system of Zijinshan area. Acta. Geosci. Sin. 26, 127–136 (in Chinese with English abstract).
Zhang, D.Q., Li, D.X., Feng, C.Y., Dong, Y.J., 2001. The temporal and spatial framework of the Mesozoic magmatic system in Zijinshan area and its geological significance. Acta. Geosci. Sin. 22, 403–408 (in Chinese with English abstract).
Zhang, D.Q., Li, D.X., Zhao, Y.M., Chen, J.H., Li, Z.L., Zhang, X.K., 1991. The Zijinshan deposit: the frist example of quartz-alunite type epithrmal deposit in the continent of China. Geol. Rev. 37, 481–491 (in Chinese with English abstract).
Zhang, D.Q., She, H.Q., Li, D.X., Feng, C.Y., 2003. The porphyry-epithermal metallogenic system in the Zijinshan region, Fujian Province. Acta. Geol. Sin. 77, 253–261 (in Chinese with English abstract).
Zhang, D.Q., Li, D.X., Zhao, Y.M., Chen, J.H., Li, Z.L., Zhang, K.Y., 1992. Alteration and mineralization zoning of the Zijinshan copper-gold deposit: Ministry of Geology and Mineral Resources of P.R. China. 1–77 (in Chinese with English abstract).
Zhang, J., Deng, J., Chen, H.Y., Yang, L.Q., Cooke, D., Danyushevsky, L., Gong, Q.J., 2014. LA-ICP-MS trace element analysis of pyrite from the Chang'an gold deposit, Sanjiang region, China: implication for ore-forming process. Gondwana Res. 26, 557–575.
Zhang, J.Z., 2013. Geology, exploration model and practice of Zijinshan ore concentrated area. Miner. Depos. 32, 757–766 (in Chinese with English abstract).
Zhao, H.X., Frimmel, H.E., Jiang, S.Y., Dai, B.Z., 2011. LA-ICP-MS trace element analysis of pyrite from the Xiaoqinling gold district, China: implications for ore genesis. Ore Geol. Rev. 43, 142–153.
Zhao, X.L., Mao, J.R., Chen, R., Xu, N.Z., 2008. SHRIMP zircon dating of the Zijinshan pluton in southwestern Fujian and its implications. Geol. China 35, 590–597 (in Chinese with English abstract).
Zhong, J., Chen, Y.J., Qi, J.P., Chen, J., Dai, M.C., Li, J., 2017. Geology, fluid inclusion and stable isotope study of the Yueyang Ag-Au-Cu deposit, Zijinshan orefield, Fujian Province. China. Ore Geol. Rev. 86, 254–270.
Zhong, J., Chen, Y.J., Chen, J., Li, J., Qi, J.P., Dai, M.C., 2011. Fluid inclusion study of the Luoboling porphyry Cu-Mo deposit in the Zijinshan orefield, Fujian Province. Acta Petrol. Sin. 27, 1410–1424 (in Chinese with English abstract).
Zhong, J., Chen, Y.J., Chen, J., Qi, J.P., Dai, M.C., 2018. Geology and fluid inclusion geochemistry of the Zijinshan high-sulfidation epithermal Cu-Au deposit, Fujian Province, SE China: implication for deep exploration targeting. J. Geochem. Explor. 184, 49–65.
Zhong, J., Chen, Y.J., Pirajno, F., Chen, J., Li, J., Qi, J.P., Li, N., 2014. Geology, geochronology, inclusion and H-O isotope geochemistry of the Luoboling Porphyry Cu-Mo deposit, Zijinshan Orefield, Fujian Province. China. Ore Geol. Rev. 57, 61–77.
Zhou, H.Y., Sun, X.M., Cook, N.J., Lin, H., Fu, Y., Zhong, R.C., Brugger, J., 2017. Nano- to micron-scale particulate gold hosted by magnetite: a product of gold scavenging by bismuth melts. Econ. Geol. 112, 993–1010.
Zhou, H.Y., Sun, X.M., Fu, Y., Lin, H., Jiang, L.Y., 2016. Mineralogy and mineral chemistry of bi-minerals: constraints on ore genesis of the beiya giant porphyry-skarn gold deposit, southwestern china. Ore Geol. Rev. 79, 408–424.
Zhou, S., Chen, H.S., 1996. Geochronology and geological significance of the Zijinshan copper-gold deposit. Bull. Mineral Petrol. Geochem. 15, 216–219 (in Chinese with English abstract).